Research Article

Origin, transport and deposition of aerosol iron to Australian coastal waters

Morgane M. G. Perron [a,*], Bernadette C. Proemse [a,c], Michal Strzelec [a], Melanie Gault-Ringold [b], Philip W. Boyd [a,b], Estrella Sanz Rodriguez [c], Brett Paull [c], Andrew R. Bowie [a,b].

[a] Institute for Marine and Antarctic Studies, University of Tasmania, Battery Point, Tasmania, Australia

[b] Antarctic Climate and Ecosystems CRC, University of Tasmania, Battery Point, Tasmania, Australia

[c] Australian Centre for Research on Separation Science (ACROSS), School of Natural Sciences, University of Tasmania, Sandy Bay Tasmania 7001, Australia

* Correspondence: Morgane M. G. Perron

morgane.perron@utas.edu.au

20 Castray Esplanade, Battery Point 7004, Tasmania, Australia

+61 3 6226 2509 (phone)

Abstract

Australia is a major source of Fe-laden dust to the anemic marine phytoplankton in the Southern Ocean and to Southern Hemisphere (SH) low latitudes diazotrophic bacteria. However, the paucity of observations and laboratory experiments on SH aerosols biases model predictions of atmospheric Fe deposition to the southern oceans and the subsequent response of ocean productivity. As a result of an extensive shipboard aerosol sampling effort, this study presents laboratory measurements of aerosol Fe concentrations, solubilities and fluxes and analysis of chemical tracers, highlighting the large heterogeneity between aerosol Fe sources in 5 coastal regions around Australia. While dust-sourced high Fe loadings and low Fe solubilities (5%) dominated aerosols from the western coasts of Australia, much lower Fe concentrations but greater Fe solubilities (10.5% and 13%) were measured in aerosols along the east coast and attributed to solubility-enhancing atmospheric reactions with anthropogenic pollutants. Finally, surprisingly high aerosol Fe solubilities (>20%) in northern Australia aerosols were associated with direct emissions or atmospheric reactions with bushfire emissions at tropical latitudes, which accounted for 49% of the total (sum) atmospheric dry deposition flux of labile Fe measured across the continent's surrounding seawaters in this study.

Keywords: "labile iron", "dust", "anthropogenic pollutants", "bushfire", "solubility", "Southern Hemisphere"

1 Introduction

The atmospheric pathway carries a significant amount of essential micro-nutrients such as iron (Fe) to anemic phytoplankton in High Nitrate Low Chlorophyll (HNLC) marine regions (Boyd and Ellwood, 2010) and to diazotrophic bacteria in subtropical waters (Moore et al., 2013). However, only a fraction of atmospheric Fe is soluble in seawater (Baker and Croot, 2010), of which only parts are bioavailable to marine biota (Jickells and Moore, 2015). Laboratory measurements of Fe solubility have often been used as a proxy for bioavailable Fe in aerosols.

Despite the recent effort to include aerosol solubility in international data bases such as the GEOTRACES Intermediate Data Product 2017 (Schlitzer et al., 2018) and the SOLAS Implementation Products (Brévière and the SOLAS Steering Committee (eds.), 2016), large discrepancies between experimental protocols (various leaching solutions, reaction pH and leaching time) prevent an accurate comparison of the solubility data between studies (Perron et al., 2020). Seawater solubility of Fe from aerosols is complex as it depends on external environmental factors such as temperature, humidity, atmospheric acidity, and sunlight and on the particle's own properties such as the source, size, and geochemical and mineralogical composition (Hettiarachchi et al., 2019).

Mineral aerosols (or "dust") dominate total atmospheric Fe emissions (Jickells and Moore, 2015), although dust generally displays very low Fe solubilities of less than 1% (Jickells and Moore, 2015). However, dust mineralogy is critical when assessing the global impact of dust deposition to the ocean as Fe-rich oxides and hydroxides (e.g., hematite, goethite, magnetite or ferrihydrite) generally only contain less than 0.01% soluble Fe compared to lower Fe bearing aluminosilicates and clay minerals which contain up to 5% soluble Fe (Journet et al., 2008).

Such low soluble Fe content of mineral aerosols contradicts the wide range of aerosol Fe solubilities (0.01% to 80%) reported (Mahowald et al., 2005). Therefore, other atmospheric

sources of more soluble Fe have been suggested, including anthropogenic emissions of biomass and fossil fuel combustion (Sedwick et al., 2007), shipping activity (Ito, 2013), fires (Guieu et al., 2005) and, regionally, volcano eruptions (Achterberg et al., 2013). Indeed, oil and coal fly ashes have a high total Fe content (80% and 25%, respectively), of which 7% and 15% may be soluble (Schroth et al., 2009; Wang et al., 2015). Consequently, anthropogenic aerosols have often been found to dominate the deposition of soluble atmospheric Fe to seawater (Sholkovitz et al., 2009). Biomass burning emissions have also been shown to contain a high fraction of soluble Fe up to 22% (Ito and Shi, 2016) or 46% (Oakes et al., 2012), which may also represent an important source of aerosol Fe near low latitude regions of the Southern Hemisphere (SH) where large bushfires seasonally occur (Winton et al., 2016). Modelling studies has attributed 79% of the soluble Fe deposition to the global ocean to combustion emissions (Wang et al., 2015) and up to 50% in remote HNLC areas (Luo et al., 2008; Scanza et al., 2018).

The solubility of mineral Fe has been observed to increase during atmospheric transport. Such solubility-enhancing mechanisms include "ageing" of airborne particles after multiple evaporation and condensation cycles within clouds (Baker and Croot, 2010; Shi et al., 2015); chemical reactions with low pH anthropogenic pollutants like sulfuric and nitric acids (Myriokefalitakis et al., 2018); or soluble complex formation with airborne organic ligands such as oxalate (Ingall et al., 2018). The latter proton-promoted and ligand-mediated reactions may enhance mineral Fe solubility by up to 75% when acting in conjunction (Johnson and Meskhidze, 2013), although they are both suppressed or buffered in the presence of carbonate minerals (Ingall et al., 2018). The presence of volcanic ash and biomass burning particles was also found to enhance mineral Fe solubility (Myriokefalitakis et al., 2018).

The SH only accounts for a few, sparsely located dust source regions (Mackie et al., 2008; Wagener et al., 2008) such as the 'outback' Australia in the center of the continent, which has often been suggested to dominate mineral aerosol deposition to the Southern Ocean (SO) south

of 45 °S (Ito and Kok, 2017; Revel-Rolland et al., 2006). Australia may also constitute an important source of airborne Fe to the highly diverse tropical to temperate marine ecosystems neighbouring the country, although very few studies have previously investigated aerosol Fe in this region. This lack of field observations and laboratory studies limits our understanding of the atmospheric cycling of Fe and also biases modelling predictions on aerosol deposition to SH waters (Wang et al., 2015), which have often been based on northern hemisphere parameterisations. Thus additional field observations are needed to refine and validate models prepresentation of atmospheric Fe biogeochemical cycling (Mackie et al., 2008). In the context of rapid climate change, there is an increasing need for observations on aerosol cycling and atmospheric processing in the SH (Scanza et al., 2018) in order to better understand today's processes and help predict and prepare for future environmental conditions.

This study presents results from an extensive ship-board atmospheric sampling effort around Australia, including observational and experimental data on aerosol Fe sources, concentrations, solubilities and deposition fluxes in the SH. Spatial variability in atmospheric delivery of Fe to five very distinct marine regions around Australia was found to be high, likely leading to varying impacts on regional marine ecosystems. We anticipate that this new dataset will significantly improve aerosol deposition models predicting SH processes.

2 Materials and methods

2.1. Study area

The Australian continent has a highly heterogeneous climate and associated diverse ecosystems, distributed across 8 states and territories subject to diverse land use and marine area management policies (McNeill, 1994). The central 'outback' constitutes a vast dust source

and includes geological basins in the east and sandy deserts in the west (Mackie et al., 2008). Australia's atmospheric circulation is divided into three major pathways, flowing south-eastwards into the Tasman Sea, north-westwards into the Indian Ocean and along the south coast of Western Australia into the Great Australian Bight (Baddock et al., 2015; Bowler, 1976). These "dust paths" are intensified over large dust storm events (Gabric et al., 2010). Despite the occurrence of seasonal monsoons at tropical latitudes, the overall climate is extremely dry (Prospero et al., 2002) and prone to severe bushfires which contribute to atmospheric combustion emissions. Australia's population is generally small and therefore its anthropogenic emissions to the atmosphere relatively small compared to populated areas of the northern hemisphere. This study investigates aerosol Fe deposition to five distinct marine regions adapted from the Australian government "State of the Environment" (SoE) marine areas (Evans et al., 2016) in order to match our sampling tracks and observations. Fig 1 displays all five regions and their potential aerosol sources.

The "Northern Marine Region" (NMR) expands from Broome (Western Australia) to the north of the Great Barrier Reef (GBR) marine park. The NMR climate is extremely hot and dry throughout most of the year which frequently triggers widespread bushfires in the local grassland, savanna and shrubland (Mallet et al., 2017). Contrastingly, the tropical monsoon causes large river discharges into the well-mixed shallw waters of the Gulf of Carpentaria (Smith et al., 2014), inducing a summer peak (up to 1.4 g C m^{-2} d^{-1}) in the gulf's primary productivity (Condie and Dunn, 2006). The topsoil primarily features illite and kaolinite aluminosilicates (Viscarra Rossel, 2011). The capital city of Darwin is the sole modest source of urban emissions to the NMR atmosphere including industries and fishery activities, but also offshore exploitations in the adjacent Joseph Bonaparte gulf. In shallow waters, high turbidity

and relatively low concentrations of nitrate (<0.3 micro mole per liter) primarily limit the development of local diatoms and nitrogen-fixing cyanobacteria (Condie and Dunn, 2006).

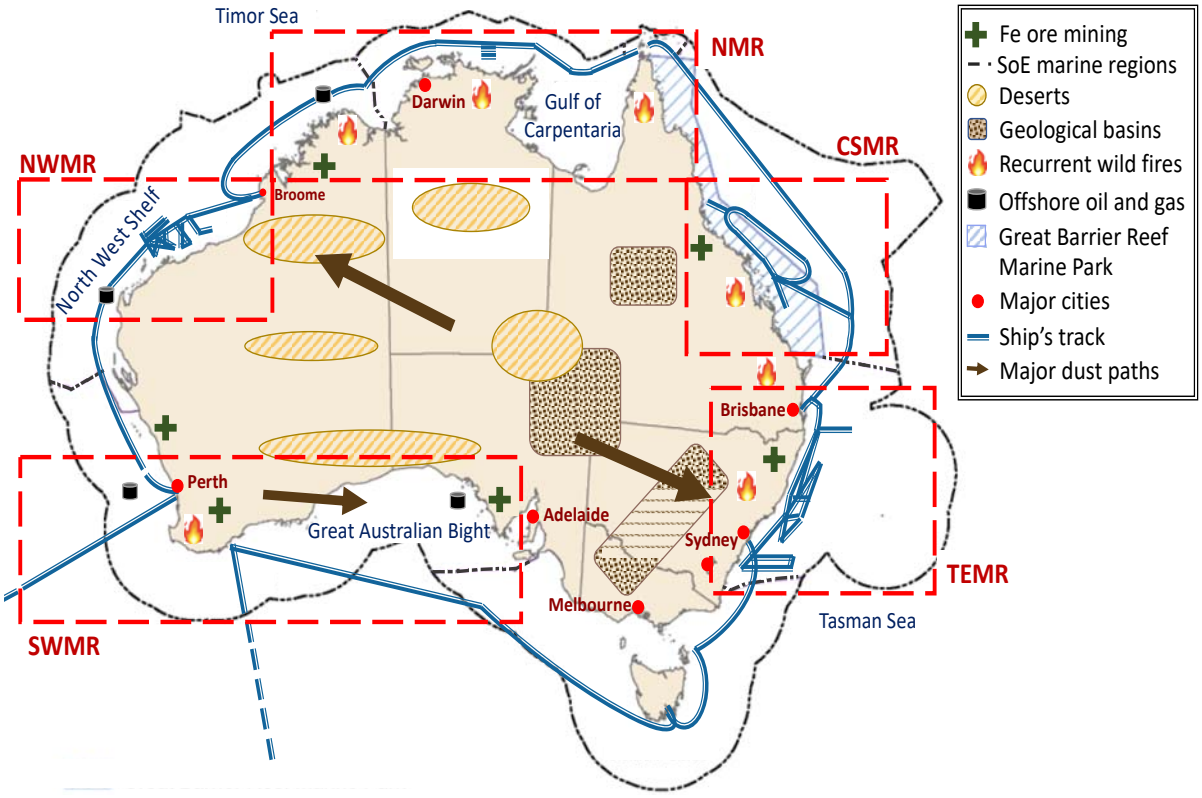

Fig 1. Schematic of the five Australia marine regions described in this study (red dashed rectangles), namely the North Marine Region (NMR), the North West Marine Region (NWMR), the South West Marine Region (SWM), the Coral Sea Marine Region (CSMR) and the Temperate East Marine Region (TEMR) which were adapted from the Australian government SoE (black dashed line). Aerosol sources and major dust paths are explained in the legend. The blue line represents all combined voyage's tracks.

The "Coral Sea Marine Region" (CSMR) spreads across the southern half of Queensland coastlines, including the GBR marine park and the neighbouring waters of the Coral Sea. Outside El Niño–Southern Oscillation years, trade winds dominate the CSMR atmospheric circulation. Summer rainfalls generate riverine outflows (Blondeau-Patissier et al., 2011) which erode kaolinite and hematite minerals from the highland basaltic rocks and smectite

minerals from lowlands (Viscarra Rossel, 2011) into the coastal waters. Queensland coasts are moderately populated, contributing to industrial, shipping, tourism and household-associated emissions to the atmosphere. Year-round low primary productivity was reported in the CSMR (0.35 to 0.55 g C m^{-2} d^{-1}) due to persistent nitrate limitation of the local nano- and pico-plankton, especially in the oligotrophic outer shelf waters (Condie and Dunn, 2006). Irregular nutrient inputs from riverine discharge or seasonal tropical cyclones sporadically feed small diatom blooms in the GBR waters.

The "Temperate East Marine Region" (TEMR) spreads from Brisbane to the south of New South Wales, and includes both Lord Howe and the Norfolk islands. Four seasons characterize the subtropical to temperate climate of the TEMR. The highly diversified vegetation of broadleaf and mixed forests on the coasts and grassland and savanna inland suffer from frequent summertime fires (Paton-Walsh et al., 2014). Soil geology resembles that of the CSMR (Viscarra Rossel, 2011) although the high density of population significantly modified the coastal landscape of the TEMR, resulting in significant anthropogenic emission to the atmosphere in this region. Averaged summer primary productivity is rather low (0.45 g C m^{-2} d^{-1}) in the northern Tasman Sea (Condie and Dunn, 2006) due to wide-spread nitrogen limitation which is opportunistically relieved in the events of dust storms, coastal upwellings supply (Ellwood et al., 2018) or within EAC-separating eddies (Radke et al., 2017). An additional co-limitation by Fe and P was shown to affect diazotroph species growth capacity in the TEMR (Ellwood et al., 2018).

The southern Tasman Sea marine region was not investigated in this study. However, the Fe-limited marine phytoplankton near the subantarctic zone (Bowie et al., 2009) may disproportionately respond to atmospheric Fe supply from Australia (Mahowald et al., 2005).

The "South West Marine Region" (SWMR) encompasses the city of Perth as well as the Great Australian Bight basin. This region displays temperate to subtropical climate and

landscape (Smith et al., 2014). The southern coast features a unique soils made of limestones and calcareous sands, including smectite and illite and goethite minerals, whereas west coast soils are primarily made of hematite oxides, kaolinite and quartz (Viscarra Rossel, 2011). The SWMR population is gathered around Perth and contributes atmospheric emissions from industries, recreational vessel activity, commercial fisheries; and offshore oil rigs. The SWMR primary productivity is though to be rather low, with an average summer rate of 0.4 g C m^{-2} d^{-1} reported in the Great Australian Bight. Nutrient input from the shelf seasonally feeds the nitrogen limited diatoms and small copepods communities in the local waters (Condie and Dunn, 2006).

The "North West Marine Region" (NWMR) comprises the northern part of Western Australia coasts up to Broome (Pilbara and southern Kimberley regions). This wild and dry region includes deserts and arid shrublands in the south and bushfire-prone grassland and savanna in the tropics (Mallet et al., 2017; Smith et al., 2014). Soil geology is dominated by kaolinite in addition to illite on the coast and hematite in the central plateau (Viscarra Rossel, 2011; Viscarra Rossel and Chen, 2011). The NWMR is quasi-deserted and therefore accuonts for very low anthropogenic emissions from mining and tourism. The North West Shelf of Australia is a highly productive marine region (>1.45 g C m^{-2} d^{-1} in winter) which relies on surface water nutrient recycling (Condie and Dunn, 2006), a strong tidal system (internal mixing) and local upwellings (Blondeau-Patissier et al., 2011), the latter phenomenon strengthening over El Niño-Southern Oscillation years (Radke et al., 2017).

2.2. Sampling

Aerosol samples were collected during multiple oceanographic voyages aboard the Research Vessel Investigator (Marine National Facility, Australia) using 47 mm punches of

204 acid cleaned Whatman 41 (W41) cellulose filters as recommended by the GEOTRACES
205 Cookbook v3 (Cutter et al., 2017; Morton et al., 2013). The ship's track is displayed in Fig 1
206 and a picture of the sampling manifold is available in the Supplementary material Fig S1. Air
207 was pumped through a polished stainless-steel pipe running along the ship's foremast and into
208 a filtration manifold housed in a High Efficiency Particulate Air (HEPA)-equipped laminar
209 flow hood, using either Teflon or anti-static conductive silicone tubing (Kenelec Scientific®)
210 to minimise potential particle loss within the manifold tubing. In order to avoid contamination
211 from the ship's exhaust, the manifold's pumps were automated to activate for a wind speed
212 between 8 to 80 km h^{-1} and a wind sector relative to the bow (270º - 90º), using the vessel's
213 meteorological data. Aerosol sampling was performed for 18 to 60 h so that a minimum volume
214 of 20 m^3 of air was filtered through each sample. After collection, sample filters were folded
215 in half and stored frozen in double sealed bags. Additional information on the sampling system
216 is available in Perron et al. (2020) (Perron et al., 2020). Acid washed W41 procedural blanks
217 were mounted on the non-running filtration manifold for 2 min and were used to correct aerosol
218 measurements for trace metal background. The supplementary material Table S2 provides a
219 log-sheet of all 44 aerosol samples collected.
220

221 *2.3. Sample processing and analysis*

222 All chemicals used were ultra-high purity Baseline (Seastar chemicals®) or in-house sub-
223 boiled distilled acids. Laboratory trace metal work was carried out in a positive pressured class
224 6 clean room, in an HEPA-filtered class 5 laminar flow hood wearing clean garments and nitrile
225 gloves and following GEOTRACES 'Cookbook' procedures (Cutter et al., 2017).
226 Aerosol samples were thawed at room temperature and processed through a three-step
227 leaching protocol to define the fractions of soluble ($S_{Fe\%}$) and labile ($L_{Fe\%}$) Fe as well as the

total Fe (T_{Fe}) in aerosols (Perron et al., 2020). Briefly, soluble Fe (S_{Fe}) was extracted by an instantaneous flow-through leach using 50 mL of ultra-high purity water (UHPW) under vacuum (Buck et al., 2006). The same filter was immediately transferred into a centrifuge tube, soaked for one hour in 10 mL of ammonium acetate (1.4 M, pH 4.7) and centrifuged (Baker et al., 2007). Labile Fe (L_{Fe}) is defined as the sum of the first two leaches. Finally, the remaining filter was digested using a mixture of HF and HNO_3 for 12 h at 120 °C (Morton et al., 2013). The sum of the three leaches defines the total Fe content (T_{Fe}) in aerosols. Fe concentrations were expressed in nanogram of Fe per meter cube (ng m^{-3}) of air filtered. Aerosol Fe fractional solubility ($S_{Fe\%}$ or $L_{Fe\%}$) was calculated as the ratio of S_{Fe}/T_{Fe} or L_{Fe}/T_{Fe} measured in aerosols, expressed as a percentage. Leachates and digests were diluted to 1% and 2% nitric acid (HNO_3), respectively, and 100 µg/kg of indium (In) was added as an internal standard. Analysis was undertaken by Sector Field Inductively Coupled Plasma-Mass Spectrometry (SF-ICP-MS, Thermo Fisher Scientific ELEMENT 2) within 3 days of sample preparation (Bowie et al., 2010). Refrence material digestion (<3 µm Arizona Test Dust, Powder Technologies Inc® and GeoPT13 loess, International Association of Geoanalysts) provided near 100% recovery for all trace metals analysed in this study (Perron et al., 2020).

2.4. Dry Fe deposition flux estimation

In order to compare our observational study with modelling studies, we calculated the dry deposition fluxes (F) of labile and total Fe using the following equation (1):

$$F_{dry} = C_{Fe} * Vd \quad (1)$$

where the measured concentrations of Fe in aerosol (C_{Fe}=L_{Fe} or T_{Fe}) was multiplied by a dry deposition velocity constant Vd. Because Vd varies greatly with the size of aerosols and atmospheric conditions such as humidity and wind speed, a constant value of 2 cm s^{-1} was used

252 in this study, allowing comparison with in previous studies (Baker et al., 2016; Duce et al.,
253 1991; Winton et al., 2016).

254 *2.5. Predominant atmospheric circulation*

255 A three-day air-mass back-trajectory analysis was undertaken using the Hybrid Single
256 Particle Lagrangian Integrated Trajectory (HYSPLIT, reanalysis, Air Resources Laboratory
257 NOAA) model (Stein et al., 2015) in order to identify dominant sources of aerosols to each
258 region considered. Air-masses back trajectories were drawn at 10 and 100 meters high to assess
259 variations in the marine boundary layer. However, atmospheric circulation is complex over a
260 sampling period of several days on a moving platform like a ship. Therefore, HYSPLIT
261 observations were combined to external measurements of atmospheric radon (^{222}Rn), a
262 lithogenic tracer used to indicate the time scale an air mass last encountered land. Atmospsheric
263 radon concentration was continuously measured during all voyages from the same air inlet as
264 the aerosol sampling system but using an independent 700L two-filter radon detector. In this
265 study, air-masses presenting a ^{222}Rn signature below 200 mBq m^{-3} were considered of a
266 predominant marine origin (Chambers et al., 2018).
267

268 *2.6. Enrichment factor*

269 The origin of aerosols is a key controller on Fe solubility (Ingall et al., 2018). Enrichment
270 factors (EF) were calculated for each sample in order to discriminate Fe from anthropogenic
271 pollution over natural dust (Shelley et al., 2015). EF was defined as the mass ratio of total Fe
272 to aluminum (Al) measured in a sample divided by the same ratio measured in the Earth' upper
273 continental crust (McLennan, 2001). An EF for Fe (EF_{Fe}) equal to 1 indicates a dominant dust
274 origin. Similarly, the EFs of vanadium (V), EF_V, (Sholkovitz et al., 2009) and lead (Pb), EF_{Pb},
275 (Shelley et al., 2017) were used to fingerprint pollution from heavy oil combustion (including

shipping) or from fuel combustion emissions, respectively. For all three trace metals, an EF exceeding the threshold value of 10 (Shelley et al., 2017) highlighted significant enrichment in the samples.

2.7. Biomass burning events

Levoglucosan, a monosaccharide anhydride, is commonly used as a tracer for biomass burning in aerosols as it only forms during high temperature combustion of cellulose. Levoglucosan quantitation was performed on duplicate W41 filters, after a short 20 min ultrasonic extraction in UHPW, using ion chromatography - triple quadrupole tandem mass spectrometry (IC-TSQ-MS) (Sanz Rodriguez et al., 2019). As no duplicate filters were available for samples from the GBR and NMR and for a few samples of the TEMR and NWMR, the online tool Sentinel Hotspots (Wooster et al., 2012) was used as an indicator for potential fire activity over the sampling period of these samples. This tool indexed all individual high confidence (80 - 100%) bushfires observed by MODIS and VIIRS satellites at the time of aerosol sampling and in a 5º x 5º area (~ 500 km^2) around the sample mid-point location (Winton et al., 2016) thereafter mention as “fire counts”. While Sentinel Hotspot is a good indicative tool for fire activity, it is not an intrinsic measurement of a sample (like levoglucosan) and therefore may not represent the genuine aerosol content carried by a sampled air-mass.

3 Results and Discussion

3.1. Air-mass influence

298 Dominant atmospheric influence in each marine region investigated was assessed using
299 atmospheric ^{222}Rn concentration and 3-day HYSPLIT air-mass back trajectories. Data is
300 available in the supplementary materials Table S3 and Fig S4.
301
302 Air-mass back-trajectories associated with NMR aerosols mainly originated from the
303 eastern Pacific Ocean and flowed westward into the Arafura Sea. However, slightly high
304 average atmospheric ^{222}Rn concentration of 551 mBq m^{-3} measured over the aerosol sampling
305 period in the NMR slightly indicated small terrestrial inputs rather than a sole marine air
306 constituted the NMR atmosphere. Such lithogenic signature is likely to originate from Australia
307 northern coastline and from the numerous islands of the Torres Strait. Similarly, the CSMR
308 displayed a primary influence by marine wind (HYSPLIT back-trajectory) which included
309 terrestrial contribution from the local coast and potentially from Pacific islands (New
310 Caledonia, Vanuatu, and Fiji) in light of the average ^{222}Rn concentration (507 mBq m^{-3})
311 measured over the CSMR aerosol sampling time. The dominant wind pattern in NWMR arose
312 from the large central deserts of Western Australia according to HYSPLIT air-mass back
313 trajectories and to the high average atmospheric ^{222}Rn concentration of 2526 mBq m^{-3}
314 measured, typical of air-masses leaving the mainland Australia ($2000<^{222}Rn<4000$ mBq m^{-3},
315 (Chambers et al., 2018)). This NWMR dust-dominated atmospheric signature fingerprints the
316 Australian South-East Dust Path reported in previous studies (Baddock et al., 2015; Bowler,
317 1976). The SWMR atmospheric circulation displayed two different trends as one sample was
318 highly influenced by terrestrial input from central Australia (HYSPLIT and ^{222}Rn=2458 mBq
319 m^{-3}) while the other two samples air-mass back-trajetories exhibited long-range aeolian
320 transport over the SO or the Great Australian Bight associated with low atmospheric ^{222}Rn
321 concentrations (301 mBq m^{-3} and 413 mBq m^{-3}, Table S3). The small number of sample
322 collected in the SWMR (n=3) is insufficient to discriminate a dominant atmospheric source to

this region which seemed to receive both terrestrial and marine air-masses. The atmospheric circulation in the TEMR was highly variable from a sample to another. The well described North-West Dust Path (Baddock et al., 2015; Bowler, 1976) was not clearly identified from our analysis but rather as a complex mixture of air masses origins (including lithogenic, anthropogenic and marine atmospheric sources) seemed to dominate the TEMR atmospheric circulation, as suggested by HYSPLIT trajectories and by the intermediate value of atmospheric ^{222}Rn concentration (1310 mBq m^{-3}).

3.2. Aerosol Fe solubilities and concentrations

Ship-board collection of aerosols commonly occurs over a short time and is sensitive to exceptional meteorological circumstances or potential sample contamination. Therfore, Fe solubilities and concentrations measured in aerosols should be carefully interpreted, especially in regions were only a small number of samples is available (NMR and SWMR). For the same reason, median data values were chosen over average values in Table 1. Atmospheric measurements of L_{Fe} will be discussed rather than S_{Fe} as the former parameter was suggested to better represent bioavailable aerosol Fe delivered to marine phytoplankton (Perron et al., 2020). Fig 2 displays the geographic distribution of L_{Fe} and T_{Fe} measured during this study.

Table 1. Median value and range of soluble ($S_{Fe\%}$) and labile ($L_{Fe\%}$) fractions of Fe in percent (%), and total Fe concentrations (T_{Fe}) in nanogram per cubic meter (ng m^{-3}) measured in aerosols collected for the NWMR (n=12), CSMR (n=8), SWMR, TEMR (n=17), and NMR (n=4) marine regions. The ratio of S_{Fe} to the L_{Fe} concentrations (S_{Fe}/L_{Fe}, %) is also shown.

Region	NWMR	CSMR	SWMR	TEMR	NMR

$S_{Fe\%}$ [%]	**median**	**4**	**5**	**7**	**10**	**12**
	range	2 - 13	3 - 17	4 - 14	5 - 30	10 - 21
$L_{Fe\%}$ [%]	**median**	**5**	**10**	**8**	**13**	**23**
	range	3 - 15	4 - 33	7 - 16	7 - 30	22 - 29
S_{Fe}/L_{Fe} [%]	**median**	**82**	**60**	**89**	**79**	**51**
T_{Fe}	**median**	**40**	**10**	**33**	**7**	**26**
[ng m^{-3}]	range	11 - 103	4 - 61	1 - 67	1 - 29	4 - 46

346

347 Median Fe solubilities ($L_{Fe\%}$) and total concentrations (T_{Fe}) measured in aerosols showed
348 striking differences between the five studied regions (Fig 2). The highest T_{Fe} were measured
349 on the western coast of Australia, with median concentrations of 33 ng m^{-3} and 40 ng m^{-3} in
350 the SWMR and NWMR, respectively. On the contrary, east coast aerosols displayed up to 4
351 times less T_{Fe} than aerosols from the western marine regions of Australia, with T_{Fe}
352 concentrations of 10 ng m^{-3} in the CSMR and 7 ng m^{-3} in the TEMR. Median T_{Fe} concentration
353 in aerosols from the NMR showed the intermediate value of 26 ng m^{-3}.

354 Labile aerosol Fe measurements (L_{Fe}) roughly followed an inverse correlation with T_{Fe}
355 measurements in aerosols (scatter plot displayed in the supplementary material Fig S5). Indeed,
356 high loading aerosols from the two western regions were associated with low median $L_{Fe\%}$ of
357 5% and 8% for the NWMR and SWMR respectively, whereas small T_{Fe} measured in aerosols
358 from the eastern shore were associated with a larger range of $L_{Fe\%}$ and greater median
359 solubilities of 10% in the CSMR (4 - 33%) and 13% in the TEMR (7 - 30%). Generally,
360 aerosols collected in the northern half of the CSMR displayed 3-fold enhanced Fe solubility
361 compared to those collected in the southern CSMR. Surprisingly, the NMR exhibited the
362 largest L_{Fe} solubility measurements (>20%) compared to other regions (Table 1).

363 Interestingly, differences were also observed in the ratio of soluble-to-labile Fe measured
364 in aerosols across the different regions (S_{Fe}/L_{Fe}, Table 1). While S_{Fe} constituted a large
365 proportion of the L_{Fe} pool, up to 79% in the TEMR, 82% in the NWMR and 89% in the SWMR;

366 only 51% and 60% of the aerosol L_{Fe} measured in aerosols of the NMR and CSMR,
367 respectively, was S_{Fe} as defined by the 3-step leaching protocol (Perron et al., 2020). This
368 observation suggests that different sources of less soluble aerosol Fe may prevail in the NMR
369 and CSMR.
370

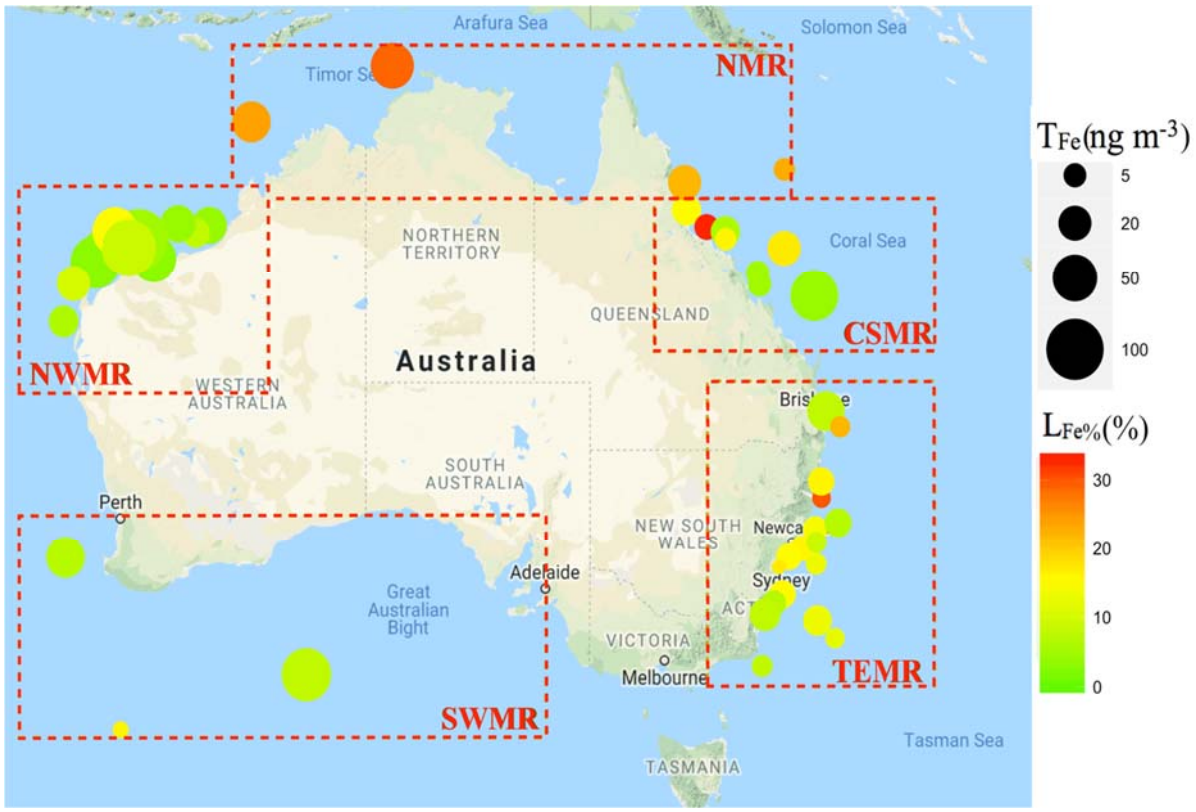

371

372 **Fig 2.** Labile Fe fraction (color scale, L_{Fe}, %) and total Fe concentration (point size, T_{Fe},
373 ng m^{-3}) in aerosols for each marine region delimited by the red dashed rectangles.
374

375 The contrast we observed between high Fe loading and poor Fe solubility in aerosols
376 collected on the Indian Ocean basin compared to low Fe loading but higher Fe solubility on
377 the Pacific Ocean east of Australia is consistent with the literature. Indeed, Strzelec and co-
378 workers measured T_{Fe} between 12 ng m^{-3} and 418 ng m^{-3} near Gingin in Western Australia
379 (Strzelec et al., 2019a) while T_{Fe} of only 29 - 214 ng m^{-3} were measured in Mission Beach,
380 northern Queensland, using the same laboratory protocol (Strzelec et al., 2019b). Greater total

aerosol Fe concentrations between 60 ng m^{-3} and 1164 ng m^{-3} were reported in aerosols at Gunn Point in the Northern Territory of Australia (Winton et al., 2016). Our atmospheric T_{Fe} measurements (0.8 – 103 ng m^{-3}, Table S5) fall within the lower end of the latter land-based field studies but they agree with shipboard studies describing aerosol T_{Fe} between 3 ng m^{-3} and 57 ng m^{-3} over the western Indian Ocean (Witt et al., 2010) and between 0.04 and 130 ng m^{-3} over the GEOTRACES GP16 section in the eastern Pacific Ocean (Buck et al., 2019). Overall, our T_{Fe} data at coastal sampling site logically fall between high land-based atmospheric Fe measurements and smaller concentrations reported in open ocean areas. This reflects the gravitational settling of large particles known to occur along the atmospheric transport away from dust emission sources (Jickells and Moore, 2015).

Laboratory experiments reported Fe solubility up to 30% when Australian sand dune was exposed to a low pH 2.15 leach (Mackie et al., 2006). Such low atmospheric pH can be reached in the presence of anthropogenic sulfur and nitrogen oxides in the atmosphere (Sholkovitz et al., 2012). Labile Fe concentrations between 0.05 and 2.7 ng m^{-3} were previously reported over the Pacific Ocean east of Australia (GEOTRACES transect GP13) (Ellwood et al., 2018) which is similar to L_{Fe} concentrations we measured in aerosols from the TEMR (0.1 - 2.5 ng m^{-3}) and CSMR (0.3 - 3.5 ng m^{-3}). Therefore, we suggest that high L_{Fe} fractions (up to 30% and 33%, respectively) measured in aerosols from the TEMR and CSMR regions may result from atmospheric processing of mineral Fe with urban emissions in such densely populated Australian coasts. Lower atmospheric Fe solubilities of 5% and 8%, respectively, measured in the NWMR and SWMR compared to other Australian regions is consistent with previous studies which reported a maximum L_{Fe} fraction of 6% in aerosols collected in Gingin, Western Australia (Strzelec et al., in prep.a) compared to up to 11% L_{Fe} in aerosols from Mission Beach, in northern Queensland (Strzelec et al., in prep.b) and L_{Fe} up to 12% reported in aerosols at Gunn Point in the Australian Northern Territory (Winton et al., 2016). Slightly

smaller Fe solubility (L_{Fe}) measured in the latter land-based studies likely relects a greater influence of less soluble coarse mineral Fe in aerosols (from the proximl dust and sand) compared to our ship-board collected aerosol samples. Indeed, Baker et al (2006) reported up to 17% L_{Fe} in aerosols collected over the southern Atlantic Ocean, which was attributed to atmospheric processing of aerosols during the atmospheric transport (Baker et al., 2006). Biomass burning and their associated emissions of acidic compounds such as oxalate was previously suggested to constitute a source of highly soluble aeolian Fe to the Northern Australia atmosphere burden (Winton et al., 2016), potentially explaining high L_{Fe} fractions (>20%) measured in our NMR aerosols.

High L_{Fe} fractions observed in aerosols from the northern CSMR and from the NMR was associated with a large contribution of less soluble Fe (NH_4Ac leach) to the L_{Fe} pool (small S_{Fe}/L_{Fe}, Table S5) compared to other regions considered. This highligjhts a common source or factor controlling such enhanced Fe dissolution of less soluble atmospheric Fe in these two regions. Shi and co-workers previously demonstrated that increasing air humidity creates a deliquescent layer around aerosols, which low pH around 2 assists Fe dissolution at the surface of aerosols and lead to enhanced Fe solubility (Shi et al., 2015). We therefore hypothesise that high atmospheric humidity in the tropical regions of Australia may lead to the higher L_{Fe} fractions measured in aerosols from the CSMR (especially the northern part) and NMR.

3.3. Dry deposition flux of total and labile Fe

Atmospheric dry deposition fluxes are displayed in Fig 3. In this study, atmospheric fluxes were calculated (equation (1) of the "Experiments" section) using a constant deposition velocity (V_d) and were therefore directly proportional to the measurements of the soluble, labile and total Fe concentrations in aerosols.

Median fluxes of T_{Fe} from aerosols, $F_{dry}(T_{Fe})$, ranged from 207.9±212.8 nanomole of Fe deposited per cubic meter of air per day (nmol Fe m^{-2} d^{-1}) in the TEMR to 1236.3±896.7 nmol Fe m^{-2} d^{-1} in the NWMR. Estimates of $F_{dry}(T_{Fe})$ were, on average, 4.5 times greater in the western marine regions of Australia (NWMR and SWMR) compared to the eastern coastal waters (CSMR and TEMR). In the NMR, $F_{dry}(T_{Fe})$ estimate displayed an intermediate value of 818.6±552.5 nmol Fe m^{-2} d^{-1}. Dry deposition fluxes of labile Fe, $F_{dry}(L_{Fe})$, ranged from 20.8±18.9 nmol Fe m^{-2} d^{-1} in the TEMR to 186.8±161.0 nmol Fe m^{-2} d^{-1} in the NMR and similar hierarchy was observed for S_{Fe} dry atmospheric flux estimates, $F_{dry}(S_{Fe})$ with values between 18.4±15.9 nmol Fe m^{-2} d^{-1} and 92.3±59.6 nmol Fe m^{-2} d^{-1} (Fig 3).

Our range of $F_{dry}(T_{Fe})$ estimates (208 - 1236 nmol Fe m^{-2} d^{-1}) fall between high T_{Fe} fluxes (377 - 12900 nmol Fe m^{-2} d^{-1}, V_d=2 cm s^{-1}) reported in a land-based aerosol study in Western Australia (Strzelec et al., 2019a) and smaller $F_{dry}(T_{Fe})$, below 100 nmol Fe m^{-2} d^{-1} (V_d=1.6 cm s^{-1}) (Buck et al., 2019) and 249 - 421 nmol Fe m^{-2} d^{-1} (V_d=2 cm s^{-1}) (Bowie et al., 2009) reported in ship-board aerosol samples from the open Pacific Ocean east of Australia and in the Southern Ocean south east of Tasmania, respectively. Our median $F_{dry}(T_{Fe})$ estimate (819 nmol Fe m^{-2} d^{-1}) to the NMR is consistent with lower $F_{dry}(T_{Fe})$ estimates of 897 nmol Fe m^{-2} d^{-1} (V_d=2 cm s^{-1}) calculated in northern Queensland, Australia (Strzelec et al., 2019b), although fluxes as high as 2000 - 36000 nmol Fe m^{-2} d^{-1} (V_d=2 cm s^{-1}) were suggested at Gunn Point, in the Northern Territory (Winton et al., 2016). Gravitational settling is known cause a significant decrease in T_{Fe} in aerosol along atmospheric transport, explaining why our $F_{dry}(T_{Fe})$ estimates logically fall between land-based calculated fluxes (at closer distance to emission source) and open ocean $F_{dry}(T_{Fe})$ estimates.

Our $F_{dry}(L_{Fe})$ flux estimates (21 - 187 nmol Fe m^{-2} d^{-1}) to coastal waters around Australia slightly exceed flux estimates of aerosol T_{Fe} of 0.5 - 25 nmol Fe m^{-2} d^{-1} (V_d=0.6 or 1.16 cm s^{-}

455 ^{1}) reported in the open south Pacific Ocean (Buck et al., 2019; Ellwood et al., 2018), below 14
456 nmol Fe m^{-2} d^{-1} (V_d=2 cm s^{-1}) in the south Indian Ocean (Witt et al., 2010) and 2 - 7 nmol Fe
457 m^{-2} d^{-1} (size-dependent V_d) in the Southern Ocean (Bowie et al., 2009). While extremely high
458 $F_{dry}(L_{Fe})$ fluxes (200 - 4000 nmol Fe m^{-2} d^{-1}) were suggested for aerosols at Gunn Point (Winton
459 et al., 2016), our average L_{Fe} flux to the NMR (187 nmol Fe m^{-2} d^{-1}) is consistent with the
460 reported average $F_{dry}(L_{Fe})$ of 213 nmol Fe m^{-2} d^{-1} in northern Queensland (Strzelec et al.,
461 2019b).
462
463 Modelling approaches are often used to calculate atmospheric deposition fluxes due to
464 their ability to better constrain particulate deposition velocity using near real-time
465 meteorological measurements and algorythms. Widely used biogeochemical models estimate
466 T_{Fe} fluxes across Australia between 2000 nmol Fe m^{-2} d^{-1} and 15471 nmol Fe m^{-2} d^{-1} (Ito et al.,
467 2019). Such discrepancies between model and field-based estimates of $F_{dry}(T_{Fe})$ reflects the
468 tendency for global models to overestimate dust transport across Australia (Ito et al., 2020).
469 However, computed flux estimates of L_{Fe} range between 15 nmol Fe m^{-2} d^{-1} and 93 nmol Fe
470 m^{-2} d^{-1} (Ito et al., 2019; Mahowald et al., 2009), which is in good agreement with estimates
471 calculated in our study.
472 One major caveat of field-based atmospheric deposition flux estimates lies in the large
473 uncertainty associated with the deposition velocity constant (V_d) whereas this parameters
474 varies according to wind speed, atmospheric humidity and the size of aerosols (Anderson et
475 al., 2016). Values from 0.6 cm s^{-1} to 2 cm s^{-1} are commonly applied to V_d (Bowie et al., 2009;
476 Ellwood et al., 2018; Witt et al., 2010), iducing a factor of 3 uncertainty between dry deposition
477 study estimates (Duce et al., 1991). New techniques using beryllium (^{7}Be) to estimate
478 atmospheric fluxes of trace metals to the ocean showed reasonable flux estimates when

compared to available measurement (Kadko et al., 2015), however, few laboratories have the facility to undertake ^{7}Be measurements.

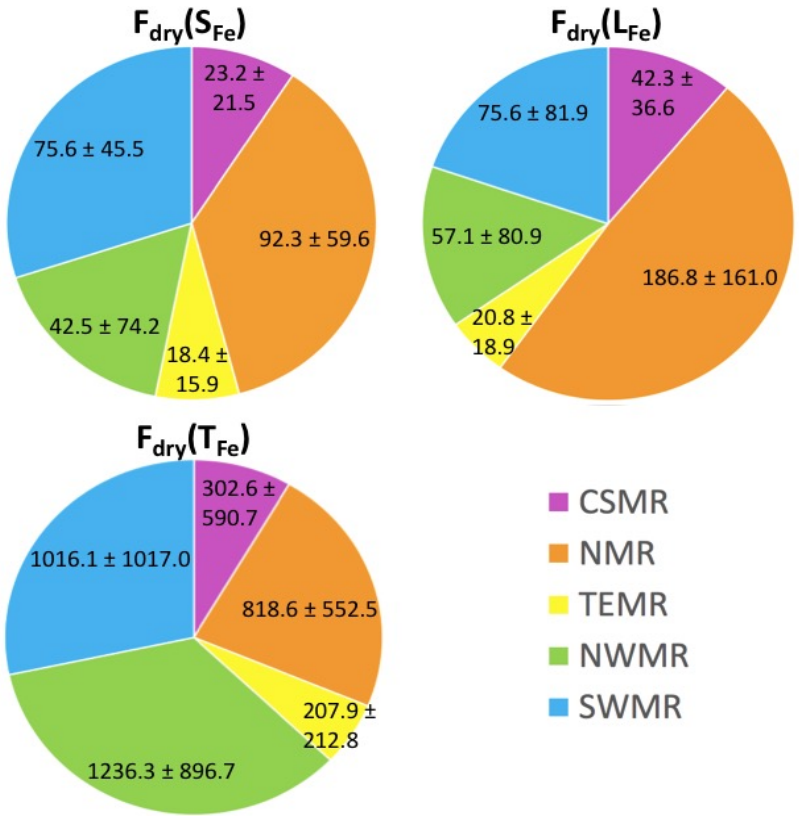

Fig 3. Proportion (pie chart) of the median atmospheric fluxes of soluble $F_{dry}(S_{Fe})$, labile $F_{dry}(L_{Fe})$ and total $F_{dry}(T_{Fe})$ Fe for each region (colour code) compared to the sum of all fluxes (%). The numerical values represent the calculated flux in nmol Fe m^{-2} d^{-1}, assuming V_d=2 cm s^{-1}, as well as the standard deviation associated to Fe measurements.

3.4. Dust versus anthropogenic influence

In order to better understand the regional variability in aerosol L_{Fe} measurements, the calculation of enrichment factors (EF) for Fe, Pb and V was used to discriminate dust source to anthropogenic emissions in the samples. Results are displayed in Fig 4 and in the

492 supplementary material Table S3. EF exceeding 10 highlighted significant “anthropogenic
493 contamination” for all three trace metals (Shelley et al., 2017).
494
495 Aerosol samples of all 5 regions displayed EF_{Fe} below 10 (Fig 4 and Table S2), indicating a
496 dominant lithogenic origin for atmospheric Fe across Australia. The three northernmost regions
497 exhibited slightly high EF_{Fe} of 2.5±1.1 in the NWMR, 2.2±2.2 in the CSMR and 2.3±1.1 in the
498 NMR which likely reflects the natural Fe enrichment (up to 50% more) in the “red” soil in
499 northern Australia compared to the average upper crust (Mahowald et al., 2005). Total aerosol
500 Fe-to-Al ratios were closer to the average upper crust value in the TEMR (EF_{Fe}=1.5±1.2) and
501 in the SWMR (EF_{Fe}=1.2±1.2). Exceptionally, higher EF_{Fe} between 4 and 8 were found in
502 individual samples (CSMR-7, TEMR-T2.3, TEMR-V4, NWMR-5, Table S3) which may be
503 attributed to local and sporadic Fe inputs from atmospheric Fe sources other than dust.
504 Atmospheric pollution from anthropogenic combustion of fossil fuel was investigated
505 using EF_{Pb} (Fig 4, Table S2). Expectedly, significant enrichment in Pb (median
506 EF_{Pb}=63.2±74.6) was found in most aerosols from the densely populated TEMR. Such Pb
507 enrichment likely reflects emissions from industries and vehicle exhaust to the urban
508 atmosphere on the south eastern Australian coast as well as power production around the city
509 of Broken Hill (Department of the Environment, 2015; Kristensen et al., 2014). Smaller but
510 significant anthropogenic input was also suggested in the slightly less urbanized CSMR as
511 indicated by a regional median EF_{Pb} of 26.4±38.4. Aerosol CSMR-7, which displayed a high
512 EF_{Fe} of 7.8 was associated with abnormal enrichment in anthropogenic Pb (EF_{Pb}=130.3)
513 compared to other CSMR aerosols suggesting that fuel combustion is a significant source of
514 Fe in this sample. Fuel combustion in Queensland mostly stem from urban areas, energy
515 production in the Bowen basin and, to a lesser extent, mining activity (Department of the
516 Environment, 2015) including Mt Isa mining town (Taylor et al., 2010). In contrast, the

517 deserted marine regions of Western Australia showed small (likely from Perth, SWMR) and
518 insignificant (NWMR) impact from anthropogenic emissions as revealed by median EF_{Pb}
519 values of 14.4±6.1 in the SWMR and 6.9±8.5 in the NWMR. High Pb content was found across
520 aerosols (n=4) from the NMR, however samples NMR-4 and NMR-5, which exhibited
521 outstanding EF_{Pb} of 383 and 459 (Table S3), largely biased the regional median EF_{Pb} of
522 217.0±224.8. Such extreme EF_{Pb} was found in the westernmost part of the NMR where
523 combustion emissions may originate from the small city of Darwin but more likely from the
524 numerous offshore gas exploitation present in the nearing Browse and Bonaparte basins
525 (Department of the Environment, 2015). Southwards atmospheric transport of wild fire or
526 pollution from Indonesia could act as a secondary Fe source to the western NMR (aerosols
527 NMR-4 and NMR-5 also displayed EF_{Fe} of 2.8 and 3.3), although no isotopic Pb measurements
528 was available to confirm such hypothesis. Atmospheric enrichment in Pb in the eastern NMR
529 (EF_{Pb} of 20 and 51) may partly stem from emissions from the very active mining town of Mt
530 Isa in northern Queensland.

531 Vanadium was used as an atmospheric tracer of oil and heavy fuel combustion in
532 aerosols (Fig 4, Table S2), which includes but is not limited to shipping emissions. The highest
533 enrichment in V was found in aerosols from the TEMR (media EF_V=50.0±41.8), emphasizing
534 the large anthropogenic influence from intense maritime traffic in this region (Department of
535 the Environment, 2015). Aerosols from the four other regions showed small signature of heavy
536 fuel or oil combustion emission, with EFV of 13.7±11.1 in the NWMR, 13.4±7.7 in the
537 SWMR, 13.5±7.7 in the NMR, and 11.3±8.9 in the CSMR. The latter signals of oil combustion
538 emissions to the atmosphere primarily reflect the omnipresence of commercial and recreational
539 shipping activity across the massive continent islnd that is Australia (Department of the
540 Environment, 2015). Strict regulations on boating tourism in the very popular GBR marine
541 park (CSMR) and Ningaloo Reef (southern NWMR) may contribute to maintaining low

shipping emissions (and therefore small V enrichment) to the atmospheric burden in these regions (Prideaux and Pabel, 2018). Offshore oil production (and the associated shipping activity) is another source of atmospheric V, especially in the Carnarvon, Browse and Bonaparte basins in the NWMR and western NMR (Ellis and Jonasson, 2002). Fremantle port and the Kwinana oil refinery, both located south of Perth, are the largest oil combustion sources in the SWMR region (Department of the Environment, 2015).

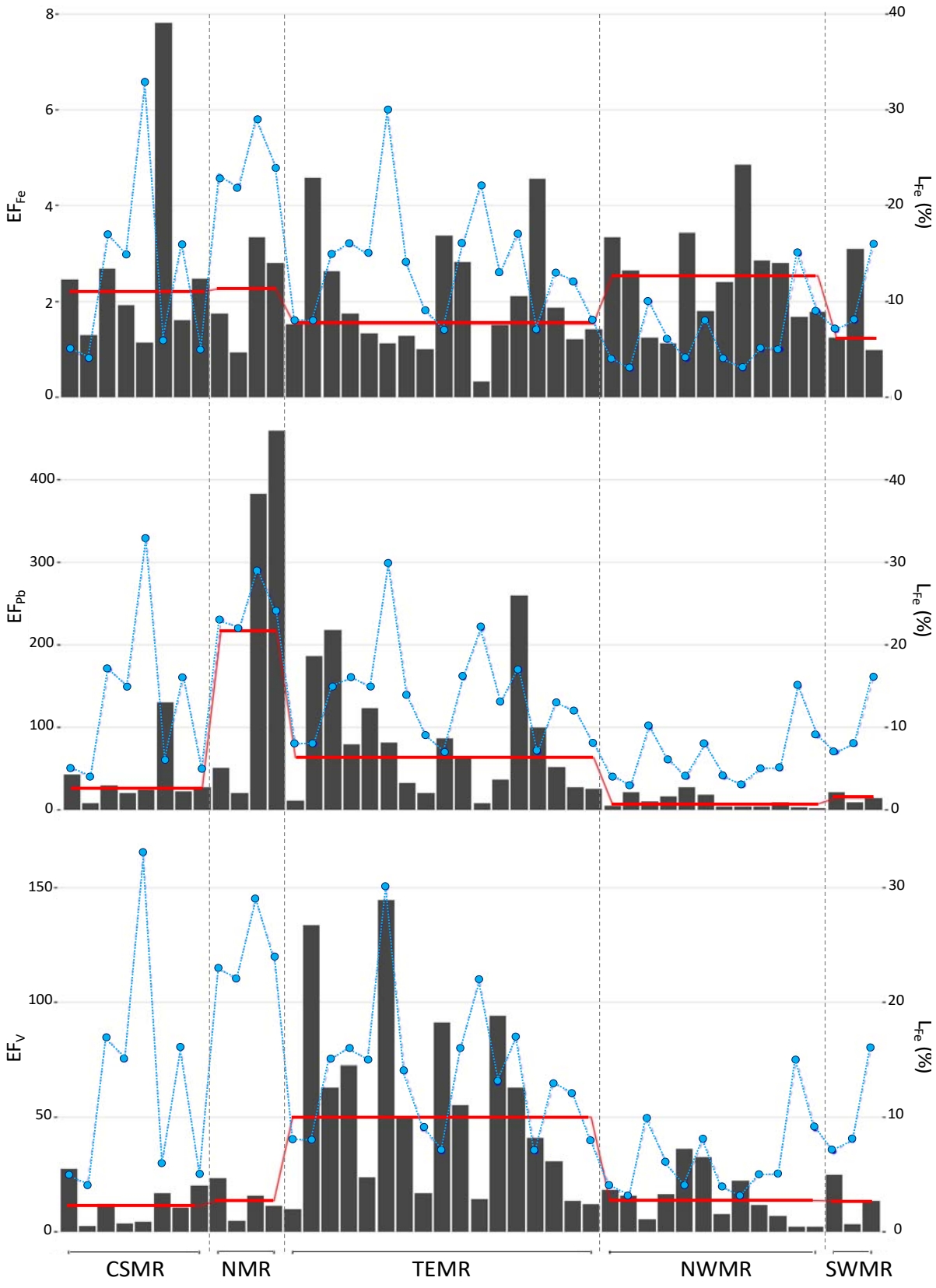

549

550 **Fig 4.** Enrichment factor (EF) of Fe, Pb and V (ratio of each trace metal to Al compared to the
551 same ratio in the upper continental crust (McLennan, 2001)) for each sample. The median EF

552 for each region (solid red line) and individual labile Fe fraction (%, blue dotted line) are also
553 displayed.
554
555 No direct relationship was observed between L_{Fe} fraction in aerosols and EFs calculus (Fig
556 4). The absence of a strong anthropogenic signal (medians EF_{Pb}=7.0 and EF_{V}=13.6) in aerosols
557 collected in the NWMR is consistent with the dust-dominated atmospheric influence suggested
558 by HYSPLIT and ^{222}Rn data analysis. Moreover, our measurements of high aerosol Fe loading
559 and low Fe solubility in NWMR aerosols are characteristic of the coarse size and strongly-
560 bound Fe-containing lattices (poor solubility) commonly reported for mineral dust (Jickells et
561 al., 2017; Srinivas and Sarin, 2013). A large contribution of emissions from industries and
562 vehicles (median EF_{Pb}=63.2) and from shipping activities (median EF_{V}=50.0) was revealed in
563 TEMR aerosols, confirming the large influence from the southeastern urban coastline
564 suggested by the air-mass back trajectory and ^{222}Rn data analysis. Anthropogenic emissions
565 are known to contain (1) more readily soluble Fe from combustion processes (Sholkovitz et
566 al., 2009) as well as (2) acidic compound (NOx, SOx) which ease mineral Fe dissolution in the
567 atmosphere (Stockdale et al., 2016). Therefore, the predominance of anthropogenic source of
568 aerosols to the TEMR atmospheric burden is likely responsible for the overall enhanced Fe
569 solubilities (median L_{Fe}=13%) measured in aerosols in this region, both through direct
570 emissions of combustion Fe and subsequent acidic processing. Combustion and shipping
571 emissions may also contribute to enhanced L_{Fe} fractions measured in aerosols from the CSMR,
572 SWMR and the NMR, although smaller EF_{Pb} and EF_{V} may imply the existence of other
573 atmospheric processes and sources to explain enhanced aerosol L_{Fe} in these regions.
574

575 *3.5. Biomass burning tracers*

Levoglucosan (Lev) was measured on "duplicate" filters in most aerosols from the TEMR, NWMR and SWMR in order to fingerprint bushfire emissions in the samples (Sanz Rodriguez et al., 2019). Half of the TEMR samples contained Lev at concentrations ranging from 6.0 to 61.2 ng m^{-3} (median Lev=11.6 ng m^{-3}), indicating a non-negligible contribution of biomass burning emissions to the atmosphere in this region. In the NWMR, only one third of aerosol samples contained detectable levoglucosan between 0.4 ng m^{-3} and 49.3 ng m^{-3} (median Lev=7.0 ng m^{-3}). The influence from biomass burning emissions to the NWMR atmospheric burden seems moderate as two samples were detected Lev concentrations below 1 ng m^{-3}, and only five aerosols (NWMR n=12) displayed between 7.0 ng m^{-3} and 49.3 ng m^{-3} of the biomass burning tracer (Table S3). All three aerosols from the SWMR contained levoglucosan at concentrations of 4.1 ng m^{-3}, 15.5 ng m^{-3} and 714.1 ng m^{-3}, indicating they were all effected by mid summer bushfires (Table S2). However, the small number of samples makes any interpretation of regional trends difficult.

The online tool "Sentinel Hotspots" was as an indicator of fire activity for aerosols collected in the NMR and CSMR, and for aerosols of the TEMR and NWMR which had no duplicate sample available for levoglucosan analysis. Sentinel Hotspot indicated bushfire events that were observed by satellite in a delimited 5ºx5º area around aerosol midpoint location and during the time of aerosol sampling. A high number of "fire counts" (>100) was reported over the sampling period of most aerosols from the NMR, suggesting a large contribution of biomass burning emissions to the atmospheric burden in this region. No fires were observed in a 5ºx5º perimeter around NMR-2 as the latter sample was collected farther offshore compared to other NMR aerosols (Table S2). However, over 200 fires were burning in Northern Australia during the collection time of NMR-2 that were not accounted for by our Sentinel Hotspot parametrisation. Similarly, biomass burning emissions were largely present in samples from the CSMR as all aerosols were detected between 19 and 745 high confidence

fires, the greater fire counts generally occurring north of 19ºS (Table S3). While a large number of fire counts (between 130 and 472) were detected in the vicinity of the remaining NWMR samples (NWMR-6, NWMR-4, NWMR-2), Sentinel Hotspot did not show a significant fire activity (0-5 fire counts) over the sampling periods of the remaining TEMR aerosols (TEMR-V3, -V6, -V10, -V12, and -V14, Table S3). Table S3 highlights some discrepancies between the use of Lev and Sentinel Hotspot as biomass burning indicators. Indeed, while levoglucosan analysis is intrinsic to a sample, Sentinel Hotspot is an indicative satellite tool which was, in this study, restricted to the observation of 80 - 100% confidence fires in a 5ºx5º perimeter around each samples.

Biomass burning emissions are known to release oxalate compounds to the atmosphere (Gillett et al., 2007), a Fe-chelating ligands which eases Fe dissolution at the surface of aerosols, often leading to enhanced atmospheric Fe solubility exceeding 10% (Ito et al., 2019). In this study, no direct relationship was observed between L_{Fe} and levoglucosan concentrations or Sentinel "fire counts" at a regional scale. Biomass burning emissions are omnipresent across Australia, with year-round fire activity at tropical latitudes in Australia but a fire season restricted to spring and summer in the southern regions (Paton-Walsh et al., 2014; Smith et al., 2014).

Aerosol sampling in the TEMR occurred in early spring (Table S2), which sets the beginning of the fire season (including controlled hazard reduction burns) in the south eastern coastal forests of Australia (Paton-Walsh et al., 2014). Therefore, enhanced L_{Fe} solubility in aerosols from the TEMR can be attributed to coastal emissions (HYSPLIT and ^{222}Rn) of natural (Lev analysis) and anthropogenic (EF study) combustion particles, either via direct emission of pyrogenic Fe or subsequent atmospheric processing. Combustion emissions are commonly associated with smaller atmospheric Fe loading (Sedwick et al., 2007) as well as fine mode

(<1 μm) aerosols (Hamilton et al., 2019). Our observation of overall low T_{Fe} concentrations measured in TEMR aerosols are therefore consistent with a predominance of anthropogenic (and, to a lesser extent, bushfires) source(s) in this region. Despite that the primary atmospheric influence for NWMR aerososl is desert dust from central Western Australia, two samples (NWMR-8 and NWMR-12) which displayed abnormally high Fe solubilities (L_{Fe}>10%) also displayed non negligible Lev concentrations of 0.8 ng m^{-3} and 49.3 ng m^{-3}. We therefore suggest that biomass burning can sporadically act as a secondary source of more soluble Fe to the NWMR.

Sentinel Hotspot analysis highlighted a widespread occurrence of large fires over our aerosol sampling campaigns in Australia's tropicals (NMR and northern CSMR). In addition to significant human emissions (EF study), we suggest that biomass burning represent another important source of readily soluble aerosol Fe and/or solubility-enhancing aeolian particles to the (northern) CSMR and the NMR, further explain high aerosol Fe solubilities (>15% and >22%, respectively) measured in these two regions. This observation agrees with previous studies suggesting an important role of bushfire emissions to the atmosphere in the northern region of Asutralia (Mallet et al., 2017; Winton et al., 2016). The small number of samples collected in the SWMR is insufficient to provide a regional overview on aerosol Fe biogeochemistry and origin in this region. Anthropogenic emissions of fuel and oil combustion from urban and shipping activities were suggested to have small to moderate impact on the SWMR atmospheric burden (EF_{Pb}<21 and EF_{V}<25). Enhanced Fe solubility (L_{Fe}>7%) measured in the dust-dominated (^{222}Rn=2458 mBq m^{-3}) sample SWMR-1 was associated to highest Lev concentration (714.1 ng m^{-3}) measured across all aerosols, reflecting the impact of the large Waroona-Yarloop fire events (Titelius, 2016) of January 2016 on enhancing aerosol Fe solubility in this sample. Despite that samples SWMR-13 and SWMR-14 displayed predominant marine origin (HYSPLIT and ^{222}Rn analysis), small concentrations of Lev (4.1

651 and 15.5 ng m^{-3}, respectively) in these samples suggest a small influence from the south west
652 costline of Australia. It is therefore hard to discriminate wether enhance L_{Fe} solubility (16%
653 and 8%, respectively) in these two samples stem from biomass burning emissions or from an
654 extensive processing of aerosol Fe over long-range atmospheric transport (Kanakidou et al.,
655 2018).
656

657 **4 Conclusions and perspectives**

658 This study results from an unprecedented effort for ship-board aerosol sampling in the
659 coastal seawater around Australia. We highlighted the high heterogeneity in the concentration
660 and solubilities (soluble and labile) of Fe in aerosols across five marine regions of Australia.
661 Such variety of aerosol mesurements were primarily guided by differences in the dominant
662 atmospheric source(s) and potential atmospheric processing for mineral Fe in each region
663 considered. Aerosols from the Australian western coastlines (NWMR and SWMR regions)
664 mostly exhibited large quantities of Fe-rich dust from the arid central 'outback', resulting in
665 low Fe solubilities after deposition (5 and 8%). Contrarily, the densely populated eastern coasts
666 (CSMR and TEMR regions) were mostly influence by fuel and oil combustion emissions form
667 anthropogenic activities, leading to smaller aerosol Fe concentrations delivered to the western
668 Pacific Ocean but greater labile Fe fractions (10 and 13%) induced by the high soluble Fe
669 content and presence of solubility-enhancing compounds in combustion aerosols. Biomass
670 burning was omnipresent across all marine regions, however, their frequency increased in the
671 tropical seawater north of Australia (NMR and northern CSMR). Fire emissions to the
672 atmosphere are thought to contribute to the surprisingly high labile Fe fractions (>20% and
673 >15%) in aerosols from the NMR and from northern CSMR. Finally, our calculation of aerosol
674 Fe dry deposition fluxes are consistent with previsous field and modelling studies and suggest
675 a significant loss of total aerosol Fe with atmospheric settling of heavy mineral particles over

676 the atmospheric transport but also an enhanced Fe solubility likely due to increased
677 atmospheric processing. Australian coastlines and suggest that Australia is a key source of bio-
678 accessible ("labile") Fe to the Indian Ocean and to the Arafura and Timor Seas through dust
679 and biomass burnig deposition respectively.
680
681 Models are a great tool to highlight key processes for atmospheric deposition of Fe to the
682 ocean and its impact on ocean productivity and they can suggest research needs for future field
683 studies. However, flux comparison with modelling studies emphasise the need to fine-tune
684 model outputs against field observations in the Southern Hemisphere (Ito et al., submitted). A
685 better parametrization of aerosol Fe concentration and solubility in models will provide more
686 accurate estimates of aerosol deposition velocity (by the models) for use in field-based
687 estimates. In addition, large uncertainties exist between field measurements due to the lack of
688 standard aerosol leaching protocol to determine L_{Fe}. This creates large variabilities between
689 observational data which should be accounted for when comparing data between studies and
690 when using field data in models (Meskhidze et al., 2019; Perron et al., 2020).
691 The assessment of aerosol Fe wet deposition to the ocean remains technically challenging
692 due to the high episodicity of rain events. However, it was previously suggested that rainfall
693 may dominate atmospheric Fe deposition in tropical regions of the Atlantic Ocean (Baker et
694 al., 2007) and the northern Queensland coast in Australia (Strzelec et al., 2019b). Because our
695 estimates of aerosol Fe dry deposition fluxes do not account for wet Fe deposition, we suggest
696 readers to interpret fluxes reported in this study as a lower limit estimates to the bulk
697 atmospheric Fe deposition to Australia coastal waters, especially at tropical low latitude (here
698 referred to as NMR and CSMR). Additional field observations are requitred to better constrain
699 atmospheric wet deposition at different latitudes across Australia and in the open ocean.

Particle size distribution is beyond the scope of this study. However, shipboard-collected aerosols were previously reported to predominantly exist in the <10 μm size fraction for mineral dust (Baker and Jickells, 2006) and in the submicron (<30 - 280 nm) size fraction for combustion (including biomass burning) particles (Winton et al., 2016). Based on our total aerosol loading measurmenets, it seems a reasonable assumption that aerosols investigated in this study are comprised within similar size range, although future aerosol size-segregation studies would be of critical interest.

A better evaluation of the marine and atmospheric budget of Fe and other essential nutrients in Australia is still requires to better quantify the role of different source reservoirs of nutrients as well as possible (co-)limitation existing across marine communities in different marine ecosystems around Australia.

Acknowledgments

We are grateful to the officers, crew and scientists on board the R.V. Investigator (Marine National Facility) for assistance in the development of a shipboard aerosol sampling system and their assistance in aerosol collection. The Authors wish to thank the CSIRO Marine National Facility (MNF) for its support in the form of sea time on RV Investigator, support personnel, scientific equipment and data management. All data and samples acquired on the voyage are made publicly available in accordance with MNF Policy. Special acknowledgment to Ian McRobert and Peter Shanks at CSIRO for you precious help in obtaining meteorological and atmospheric data from the ship, as well as Dr Scott D. Chambers from the Australian Nuclear Science and Technology Organization (ANSTO) for precious help and advices in interpreting radon measurements aboard the R.V. Investigator. All ICP–MS analyses were undertaken at the Central Science Laboratory (CSL) at the University of Tasmania thanks to the expertise of A/Prof Ashley Townsend (ICP-MS). This paper also includes data obtained using HYSPLIT online model from the Air Resources Laboratory of the National Oceanic and Atmospheric Administration as well as using Sentinel Hotspots online tool available through Geoscience Australia.

Funding

This work was supported by an Australian Research Council Future Fellowship (FT130100037 to A.R.B.) and through the Antarctic Climate and Ecosystems Cooperative Research Centre (ACE CRC).

5 References

Achterberg, E.P., Moore, C.M., Henson, S.A., Steigenberger, S., Stohl, A., Eckhardt, S., Avendano, L.C., Cassidy, M., Hembury, D., Klar, J.K., Lucas, M.I., MacEy, A.I., Marsay, C.M., Ryan-Keogh, T.J., 2013. Natural iron fertilization by the Eyjafjallajökull volcanic eruption. Geophys. Res. Lett. 40, 921–926. https://doi.org/10.1002/grl.50221

Anderson, R.F., Cheng, H., Edwards, R.L., Fleisher, M.Q., Hayes, C.T., Huang, K.-F., Kadko, D., Lam, P.J., Landing, W.M., Lao, Y., Lu, Y., Measures, C.I., Moran, S.B., Morton, P.L., Ohnemus, D.C., Robinson, L.F., Shelley, R.U., 2016. How well can we quantify dust deposition to the ocean? R. Soc. Publ. https://doi.org/10.1098/rsta.2015.0285

Baddock, M., Parsons, K., Strong, C., Leys, J., Mctainsh, G., 2015. Drivers of Australian dust: A case study of frontal winds and dust dynamics in the lower lake Eyre basin. Earth Surf. Process. Landforms 40, 1982–1988. https://doi.org/10.1002/esp.3773

Baker, A.R., Croot, P.L., 2010. Atmospheric and marine controls on aerosol iron solubility in seawater. Mar. Chem. 120, 4–13. https://doi.org/10.1016/j.marchem.2008.09.003

Baker, A.R., Jickells, T.D., 2006. Mineral particle size as a control on aerosol iron solubility. Geophys. Res. Lett. 33. https://doi.org/10.1029/2006GL026557

Baker, A.R., Jickells, T.D., Witt, M., Linge, K.L., 2006. Trends in the solubility of iron, aluminium, manganese and phosphorus in aerosol collected over the Atlantic Ocean. Mar. Chem. 98, 43–58. https://doi.org/10.1016/j.marchem.2005.06.004

Baker, A.R., Landing, W.M., Bucciarelli, E., Cheize, M., Fietz, S., Hayes, C.T., Kadko, D., Morton, P.L., Rogan, N., Sarthou, G., Shelley, R.U., Shi, Z., Shiller, A.M., van Hulten, M.M.P., 2016. Trace Element and Isotope Deposition across the Air-Sea Interface: Progress and Research Needs. Philos. Trans. A. https://doi.org/10.1098/rsta.2016.0190

Baker, A.R., Weston, K., Kelly, S.D., Voss, M., Streu, P., Cape, J.N., 2007. Dry and wet deposition of nutrients from the tropical Atlantic atmosphere: Links to primary productivity and nitrogen fixation. Deep. Res. Part I Oceanogr. Res. Pap. 54, 1704–1720. https://doi.org/10.1016/j.dsr.2007.07.001

Blondeau-Patissier, D., Dekker, A., Schroeder, T., Brando, V., 2011. Phytoplankton dynamics in shelf waters around Australia. Aust. State Environ. 2011.

Bowie, A.R., Lannuzel, D., Remenyi, T.A., Wagener, T., Lam, P.J., Boyd, P.W., Guieu, C., Townsend, A.T., Trull, T.W., 2009. Biogeochemical iron budgets of the Southern Ocean south of Australia Decoupling of iron and nutrient cycles in the subantarctic zone by the summertime supply. Global Biogeochem. Cycles 23. https://doi.org/10.1029/2009GB003500

Bowie, A.R., Townsend, A.T., Lannuzel, D., Remenyi, T.A., van der Merwe, P., 2010. Modern sampling and analytical methods for the determination of trace elements in marine particulate material using magnetic sector inductively coupled plasma-mass spectrometry. Anal. Chim. Acta 676, 15–27. https://doi.org/10.1016/j.aca.2010.07.037

Bowler, J.M., 1976. Aridity in Australia: Age, origins and expression in aeolian landforms and sediments. Earth Sci. Rev. 12, 279–310. https://doi.org/10.1016/0012-8252(76)90008-8

Boyd, P.W., Ellwood, M.J., 2010. The biogeochemical cycle of iron in the ocean. Nature 3, 675–682.

Brévière, E., the SOLAS Steering Committee (eds.), 2016. SOLAS 2015- 2025: Science Plan and Organisation. SOLAS International Project Office, GEOMAR Helmholtz Centre for Ocean Research Kiel, Kiel, Germany.

Buck, C.S., Aguilar-Islas, A., Marsay, C., Kadko, D., Landing, W.M., 2019. Trace element concentrations, elemental ratios, and enrichment factors observed in aerosol samples collected during the US GEOTRACES eastern Pacific Ocean transect (GP16). Chem.

783 Geol. 511, 212–224. https://doi.org/10.1016/j.chemgeo.2019.01.002
784 Buck, C.S., Landing, W.M., Resing, J.A., Lebon, G.T., 2006. Aerosol iron and aluminum
785 solubility in the northwest Pacific Ocean Results from the 2002 IOC cruise.
786 Geochemistry, Geophys. Geosystems 7. https://doi.org/10.1029/2005GC000977
787 Chambers, S.D., Preunkert, S., Weller, R., Hong, S.-B., Humphries, R.S., Tositti, L., Angot,
788 H., Legrand, M., Williams, A.G., Griffiths, A.D., Crawford, J., Simmons, J., Choi, T.J.,
789 Krummel, P.B., Molloy, S., Loh, Z., Galbally, I., Wilson, S., Magand, O., Sprovieri, F.,
790 Pirrone, N., Dommergue, A., 2018. Characterizing Atmospheric Transport Pathways to
791 Antarctica and the Remote Southern Ocean Using Radon-222. Front. Earth Sci. 6, 1–28.
792 https://doi.org/10.3389/feart.2018.00190
793 Condie, S.A., Dunn, J.R., 2006. Seasonal characteristics of the surface mixed layer in the
794 Australasian region : implications for primary production regimes and biogeography.
795 Mar. Freshw. Res. 57, 569–590.
796 Cutter, G., Casciotti, K., Croot, P.L., Geibert, W., Heimburger, L.-E., Lohan, M.C., Planquette,
797 H., van de Flierdt, T., 2017. Sampling and Sample-handling Protocols for GEOTRACES
798 Cruises v.3.
799 Department of the Environment, 2015. National Pollutant Inventory Guide. Version 6.1.
800 Camberra, Australia.
801 Duce, R.A., Liss, P.S., Merrill, J.T., Atlas, E.L., Buat-Menard, P., Hicks, B.B., Miller, J.M.,
802 Prospero, J.M., Arimoto, R., Church, T.M., Ellis, W., Galloway, J.N., Hansen, L., Jickells,
803 T.D., Knap, A.H., Reinhardt, K.H., Schneider, B., Soudine, A., Tokos, J.J., Tsunogai, S.,
804 Wollast, R., Zhou, M., 1991. The atmospheric input of trace species to the world ocean.
805 Global Biogeochem. Cycles 5, 193–259. https://doi.org/10.1029/91GB01778
806 Ellis, G.K., Jonasson, K., 2002. Rough range oilfield Carnarvon Basin. Perth, WA.
807 Ellwood, M.J., Bowie, A.R., Baker, A.R., Gault-Ringold, M., Hassler, C.S., Law, C.S., Maher,
808 W.A., Marriner, A., Nodder, S., Sander, S., Stevens, C., Townsend, A.T., van der Merwe,
809 P., Woodward, E.M.S., Wuttig, K., Boyd, P.W., 2018. Insights Into the Biogeochemical
810 Cycling of Iron, Nitrate, and Phosphate Across a 5,300 km South Pacific Zonal Section
811 (153°E–150°W). Global Biogeochem. Cycles 32, 187–207.
812 https://doi.org/10.1002/2017GB005736
813 Evans, K., Bax, N.., Smith, D.C., 2016. Marine environment: Marine regions. Australia state
814 of the environment 2016, Australian Government Department of the Environment and
815 Energy, Canberra [WWW Document]. https://doi.org/10.4226/94/58b657ea7c296
816 Gabric, A.J., Cropp, R.A., McTainsh, G.H., Johnston, B.M., Butler, H., Tilbrook, B.,
817 Keywood, M., 2010. Australian dust storms in 2002–2003 and their impact on Southern
818 Ocean biogeochemistry. Global Biogeochem. Cycles 24.
819 https://doi.org/10.1029/2009GB003541
820 Gillett, R., Galbally, I., Ayers, G., Selleck, P., Powell, J., Meyer, M., Keywood, M., Fedele,
821 R., 2007. Oxalic acid and oxalate in the atmosphere.
822 Guieu, C., Bonnet, S., Wagener, T., Loÿe-Pilot, M.-D., 2005. Biomass burning as a source of
823 dissolved iron to the open ocean. Geophys. Res. Lett. 32.
824 https://doi.org/10.1029/2005GL022962
825 Hamilton, D.S., Scanza, R.A., Feng, Y., Guinness, J., Kok, J.F., Li, L., Liu, X., Rathod, S.D.,
826 Wan, J.S., Wu, M., Mahowald, N.M., 2019. Improved methodologies for Earth system
827 modelling of atmospheric soluble iron and observation comparisons using the Mechanism
828 of Intermediate complexity for Modelling Iron (MIMI v.1.0). Geosci. Model Dev.
829 Discuss. 1–54. https://doi.org/10.5194/gmd-2019-84
830 Hettiarachchi, E., Reynolds, R.L., Goldstein, H.L., Moskowitz, B., Rubasinghege, G., 2019.
831 Bioavailable iron production in airborne mineral dust: Controls by chemical composition
832 and solar flux. Atmos. Environ. 205, 90–102.

https://doi.org/10.1016/J.ATMOSENV.2019.02.037
Ingall, E., Feng, Y., Longo, A., Lai, B., Shelley, R., Landing, W., Morton, P., Nenes, A., Mihalopoulos, N., Violaki, K., Gao, Y., Sahai, S., Castorina, E., 2018. Enhanced Iron Solubility at Low pH in Global Aerosols. Atmosphere (Basel). 9, 201. https://doi.org/10.3390/atmos9050201
Ito, A., 2013. Global modeling study of potentially bioavailable iron input from shipboard aerosol sources to the ocean. Global Biogeochem. Cycles 27, 1–10. https://doi.org/10.1029/2012GB004378
Ito, A., Kok, J.F., 2017. Do dust emissions from sparsely vegetated regions dominate atmospheric iron supply to the Southern Ocean? J. Geophys. Res. Atmos. 3987–4002. https://doi.org/10.1002/2016JD025939
Ito, A., Myriokefalitakis, S., Kanakidou, M., Mahowald, N.M., Scanza, R.A., Hamilton, D.S., Baker, A.R., Jickells, T.D., Sarin, M.M., Bikkina, S., Gao, Y., Shelley, R.U., Buck, C.S., Landing, W.M., Bowie, A.R., Perron, M.M.G., Guieu, C., Meskhidze, N., Johnson, M.S., Feng, Y., Kok, J.F., Nenes, A., Duce, R.A., 2019. Pyrogenic iron: The missing link to high iron solubility in aerosols. Sci. Adv. 5. https://doi.org/10.1126/sciadv.aau7671
Ito, A., Perron, M.M.G., Proemse, B.C., Strzelec, M., Gault-Ringold, M., Boyd, P.W., Bowie, A.R., 2020. Implications of overestimates in mineral dust emissions from Australia on bioaccessible iron concentrations in aerosols over the Southern Ocean. Prog. Earth Planet. Sci. submitted.
Ito, A., Shi, Z., 2016. Delivery of anthropogenic bioavailable iron from mineral dust and combustion aerosols to the ocean. Atmos. Chem. Phys. 16, 85–99. https://doi.org/10.5194/acp-16-85-2016
Jickells, T.D., Buitenhuis, E., Altieri, K., Baker, A.R., Capone, D., Duce, R.A., Dentener, F., Fennel, K., Kanakidou, M., LaRoche, J., Lee, K.C., Liss, P.S., Middelburg, J.J., Moore, J.K., Okin, G., Oschlies, A., Sarin, M.M., Seitzinger, S., Sharples, J., Singh, A., Suntharalingam, P., Uematsu, M., Zamora, L.M., 2017. A reevaluation of the magnitude and impacts of anthropogenic atmospheric nitrogen inputs on the ocean. Global Biogeochem. Cycles 31, 289–305. https://doi.org/10.1002/2016GB005586
Jickells, T.D., Moore, M.C., 2015. The Importance of Atmospheric Deposition for Ocean Productivity. Annu. Rev. Ecol. Evol. Syst. 46, 481–501. https://doi.org/10.1146/annurev-ecolsys-112414-054118
Johnson, M.S., Meskhidze, N., 2013. Atmospheric dissolved iron deposition to the global oceans: Effects of oxalate-promoted Fe dissolution, photochemical redox cycling, and dust mineralogy. Geosci. Model Dev. 6, 1137–1155. https://doi.org/10.5194/gmd-6-1137-2013
Journet, E., Desboeufs, K. V., Caquineau, S., Colin, J.L., 2008. Mineralogy as a critical factor of dust iron solubility. Geophys. Res. Lett. 35, 1–5. https://doi.org/10.1029/2007GL031589
Kadko, D., Landing, W.M., Shelley, R.U., 2015. A novel tracer technique to quantify the atmospheric flux of trace elements to remote ocean regions. J. Geophys. Res. Ocean. 848–858. https://doi.org/10.1002/2014JC010314
Kanakidou, M., Myriokefalitakis, S., Tsigaridis, K., 2018. Aerosols in atmospheric chemistry and biogeochemical cycles of nutrients. Environ. Res. Lett. 13. https://doi.org/10.1088/1748-9326/aabcdb
Kristensen, L.J., Taylor, M.P., Odigie, K.O., Hibdon, S.A., Flegal, A.R., 2014. Lead isotopic compositions of ash sourced from Australian bush fi res. Environ. Pollut. 190, 159–165. https://doi.org/10.1016/j.envpol.2014.03.025
Luo, C., Mahowald, N., Bond, T., Chuang, P.Y., Artaxo, P., Siefert, R., Chen, Y., Schauer, J., 2008. Combustion iron distribution and deposition. Global Biogeochem. Cycles 22.

https://doi.org/10.1029/2007GB002964
Mackie, D.S., Boyd, P.W., McTainsh, G.H., Tindale, N.W., Westberry, T.K., Hunter, K.A., 2008. Biogeochemistry of iron in Australian dust: From eolian uplift to marine uptake. Geochemistry, Geophys. Geosystems 9. https://doi.org/10.1029/2007GC001813
Mackie, D.S., Peat, J.M., McTainsh, G.H., Boyd, P.W., Hunter, K.A., 2006. Soil abrasion and eolian dust production: Implications for iron partitioning and solubility. Geochemistry, Geophys. Geosystems 7. https://doi.org/10.1029/2006GC001404
Mahowald, N.M., Baker, A.R., Bergametti, G., Brooks, N., Duce, R.A., Jickells, T.D., Kubilay, N., Prospero, J.M., Tegen, I., 2005. Atmospheric global dust cycle and iron inputs to the ocean. Global Biogeochem. Cycles 19. https://doi.org/10.1029/2004GB002402
Mahowald, N.M., Engelstaedter, S., Luo, C., Sealy, A., Artaxo, P., Benitez-Nelson, C.R., Bonnet, S., Chen, Y., Chuang, P.Y., Cohen, D.D., Dulac, F., Herut, B., Johansen, A.M., Kubilay, N., Losno, R., Maenhaut, W., Paytan, A., Prospero, J.M., Shank, L.M., Siefert, R.L., 2009. Atmospheric Iron Deposition: Global Distribution, Variability, and Human Perturbations. Ann. Rev. Mar. Sci. 1, 245–278. https://doi.org/10.1146/annurev.marine.010908.163727
Mallet, M.D., Desservettaz, M.J., Miljevic, B., Milic, A., Ristovski, Z.D., Alroe, J., Cravigan, L.T., Rohan Jayaratne, E., Paton-Walsh, C., Griffith, D.W.T., Wilson, S.R., Kettlewell, G., Van Der Schoot, M. V., Selleck, P., Reisen, F., Lawson, S.J., Ward, J., Harnwell, J., Cheng, M., Gillett, R.W., Molloy, S.B., Howard, D., Nelson, P.F., Morrison, A.L., Edwards, G.C., Williams, A.G., Chambers, S.D., Werczynski, S., Williams, L.R., Winton, V.H.L., Atkinson, B., Wang, X., Keywood, M.D., 2017. Biomass burning emissions in north Australia during the early dry season: An overview of the 2014 SAFIRED campaign. Atmos. Chem. Phys. 17, 13681–13697. https://doi.org/10.5194/acp-17-13681-2017
McLennan, S.M., 2001. Relationships between the trace element composition of sedimentary rocks and upper continental crust. Geochemistry, Geophys. Geosystems 2. https://doi.org/10.1029/2000GC000109
McNeill, S.E., 1994. The selection and design of marine protected areas: Australia as a case study. Biodivers. Conserv. 3, 586–605. https://doi.org/10.1007/BF00114203
Meskhidze, N., Völker, C., Al-Abadleh, H.A., Barbeau, K., Bressac, M., Buck, C., Bundy, R.M., Croot, P., Feng, Y., Ito, A., Johansen, A.M., Landing, W.M., Mao, J., Myriokefalitakis, S., Ohnemus, D., Pasquier, B., Ye, Y., 2019. Perspective on identifying and characterizing the processes controlling iron speciation and residence time at the atmosphere- ocean interface. Mar. Chem. https://doi.org/10.1016/j.snb.2019.127065
Moore, C.M., Mills, M.M., Arrigo, K.R., Berman-Frank, I., Bopp, L., Boyd, P.W., Galbraith, E.D., Geider, R.J., Guieu, C., Jaccard, S.L., Jickells, T.D., La Roche, J., Lenton, T.M., Mahowald, N.M., Marañón, E., Marinov, I., Moore, J.K., Nakatsuka, T., Oschlies, A., Saito, M.A., Thingstad, T.F., Tsuda, A., Ulloa, O., 2013. Processes and patterns of oceanic nutrient limitation. Nat. Geosci. 6, 701–710. https://doi.org/10.1038/ngeo1765
Morton, P.L., Landing, W.M., Hsu, S.-C., Milne, A., Aguilar-Islas, A.M., Baker, A.R., Bowie, A.R.R., Buck, C.S., Gao, Y., Gichuki, S., Hastings, M.G., Hatta, M., Johansen, A.M., Losno, R., Mead, C., Patey, M.D., Swarr, G., Vandermark, A., Zamora, L.M., 2013. Methods for the sampling and analysis of marine aerosols: results from the 2008 GEOTRACES aerosol intercalibration experiment. Limnol. Oceanogr. 11, 62–78. https://doi.org/10.4319/lom.2013.11.62
Myriokefalitakis, S., Ito, A., Kanakidou, M., Nenes, A., Krol, M.C., Mahowald, N.M., Scanza, R.A., Hamilton, D.S.D.S., Johnson, M.S., Meskhidze, N., Kok, J.F., Guieu, C., Baker, A.R., Jickells, T.D., Sarin, M.M., Bikkina, S., Shelley, R.U., Bowie, A.R., Perron, M.M.G., Duce, R.A., 2018. Reviews and syntheses: The GESAMP atmospheric iron

933 deposition model intercomparison study. Biogeosciences 15, 6659–6684.
934 https://doi.org/10.5194/bg-15-6659-2018
935 Oakes, M., Ingall, E.D., Lai, B., Shafer, M.M., Hays, M.D., Liu, Z.G., Russell, A.G., Weber,
936 R.J., 2012. Iron solubility related to particle sulfur content in source emission and ambient
937 fine particles. Environ. Sci. Technol. 46, 6637–6644. https://doi.org/10.1021/es300701c
938 Paton-Walsh, C., Smith, T.E.L.L., Young, E.L., Griffith, D.W.T.T., Guérette, É.-A., Guérette,
939 A., 2014. New emission factors for Australian vegetation fires measured using open-path
940 Fourier transform infrared spectroscopy – Part 1: Methods and Australian temperate forest
941 fires. Atmos. Chem. Phys. 14, 11313–11333. https://doi.org/10.5194/acp-14-11313-2014
942 Perron, M.M.G., Strzelec, M., Gault-Ringold, M., Proemse, B.C., Boyd, P.W., Bowie, A.R.,
943 2020. Assessment of leaching protocols to determine the solubility of trace metals in
944 aerosols. Talanta 208. https://doi.org/10.1016/j.talanta.2019.120377
945 Prideaux, B., Pabel, A. (Eds.), 2018. Coral Reefs: Tourism, Conservation and Management,
946 Routledge. ed.
947 Prospero, J.M., Ginoux, P., Torres, O., Nicholson, S.E., Gill, T.E., 2002. Environmental
948 characterization of global sources of atmospheric soil dust identified with the NIMBUS 7
949 Total Ozone Mapping Spectrometer (TOMS) absorbing aerosol product. Rev. Geophys.
950 40, 1–31. https://doi.org/10.1029/2000RG000095
951 Radke, L., Nicholas, T., Thompson, P.A., Li, J., Raes, E., Carey, M.C., Atkinson, I., Huang,
952 Z., Trafford, J., Nichol, S., 2017. Baseline biogeochemical data from Australia' s
953 continental margin links seabed sediments to water column characteristics. Mar. Freshw.
954 Res. 68, 1593–1617.
955 Revel-Rolland, M., De Deckker, P., Delmonte, B., Hesse, P.P., Magee, J.W., Basile-Doelsch,
956 I., Grousset, F., Bosch, D., 2006. Eastern Australia: A possible source of dust in East
957 Antarctica interglacial ice. Earth Planet. Sci. Lett. 249, 1–13.
958 https://doi.org/10.1016/j.epsl.2006.06.028
959 Sanz Rodriguez, E., Perron, M.M.G., Strzelec, M., Proemse, B.C., Bowie, A.R., Brett, P., 2019.
960 Analysis of levoglucosan and its isomers in atmospheric samples by ion chromatography
961 with electrospray lithium cationization - triple quadrupole tandem mass spectrometry. J.
962 Chromatogr. A. https://doi.org/10.1016/j.chroma.2019.460557
963 Scanza, R.A., Mahowald, N.M., Garcia-pando, C.P., Buck, C.S., Baker, A.R., Hamilton, D.S.,
964 2018. Atmospheric Processing of Iron in Mineral and Combustion Aerosols:
965 Development of an Intermediate-Complexity Mechanism Suitable for Earth System
966 Models. Atmos. Chem. Phys. Discuss. 1, 14196. https://doi.org/10.5194/acp-2018-80
967 Schlitzer, R., Anderson, R.F., Dodas, E.M., Lohan, M.C., Geibert, W., Tagliabue, A., Bowie,
968 A.R., Jeandel, C., Maldonado, M.T., Landing, W.M., Cockwell, D., Abadie, C.,
969 Abouchami, W., Achterberg, E.P., Agather, A., Aguliar-Islas, A., van Aken, H.M.,
970 Andersen, M., Archer, C., Auro, M., de Baar, H.J., Baars, O., Baker, A.R., Bakker, K.,
971 Basak, C., Baskaran, M., Bates, N.R., Bauch, D., van Beek, P., Behrens, M.K., Black, E.,
972 Bluhm, K., Bopp, L., Bouman, H., Bowman, K., Bown, J., Boyd, P., Boye, M., Boyle,
973 E.A., Branellec, P., Bridgestock, L., Brissebrat, G., Browning, T., Bruland, K.W.,
974 Brumsack, H.J., Brzezinski, M., Buck, C.S., Buck, K.N., Buesseler, K., Bull, A., Butler,
975 E., Cai, P., Mor, P.C., Cardinal, D., Carlson, C., Carrasco, G., Casacuberta, N., Casciotti,
976 K.L., Castrillejo, M., Chamizo, E., Chance, R., Charette, M.A., Chaves, J.E., Cheng, H.,
977 Chever, F., Christl, M., Church, T.M., Closset, I., Colman, A., Conway, T.M., Cossa, D.,
978 Croot, P., Cullen, J.T., Cutter, G.A., Daniels, C., Dehairs, F., Deng, F., Dieu, H.T.,
979 Duggan, B., Dulaquais, G., Dumousseaud, C., Echegoyen-Sanz, Y., Edwards, R.L.,
980 Ellwood, M., Fahrbach, E., Fitzsimmons, J.N., Russell Flegal, A., Fleisher, M.Q., van de
981 Flierdt, T., Frank, M., Friedrich, J., Fripiat, F., Fröllje, H., Galer, S.J.G., Gamo, T.,
982 Ganeshram, R.S., Garcia-Orellana, J., Garcia-Solsona, E., Gault-Ringold, M., George, E.,

Gerringa, L.J.A., Gilbert, M., Godoy, J.M., Goldstein, S.L., Gonzalez, S.R., Grissom, K., Hammerschmidt, C., Hartman, A., Hassler, C.S., Hathorne, E.C., Hatta, M., Hawco, N., Hayes, C.T., Heimbürger, L.E., Helgoe, J., Heller, M., Henderson, G.M., Henderson, P.B., van Heuven, S., Ho, P., Horner, T.J., Hsieh, Y. Te, Huang, K.F., Humphreys, M.P., Isshiki, K., Jacquot, J.E., Janssen, D.J., Jenkins, W.J., John, S., Jones, E.M., Jones, J.L., Kadko, D.C., Kayser, R., Kenna, T.C., Khondoker, R., Kim, T., Kipp, L., Klar, J.K., Klunder, M., Kretschmer, S., Kumamoto, Y., Laan, P., Labatut, M., Lacan, F., Lam, P.J., Lambelet, M., Lamborg, C.H., Le Moigne, F.A.C., Le Roy, E., Lechtenfeld, O.J., Lee, J.M., Lherminier, P., Little, S., López-Lora, M., Lu, Y., Masque, P., Mawji, E., Mcclain, C.R., Measures, C., Mehic, S., Barraqueta, J.L.M., van der Merwe, P., Middag, R., Mieruch, S., Milne, A., Minami, T., Moffett, J.W., Moncoiffe, G., Moore, W.S., Morris, P.J., Morton, P.L., Nakaguchi, Y., Nakayama, N., Niedermiller, J., Nishioka, J., Nishiuchi, A., Noble, A., Obata, H., Ober, S., Ohnemus, D.C., van Ooijen, J., O'Sullivan, J., Owens, S., Pahnke, K., Paul, M., Pavia, F., Pena, L.D., Peters, B., Planchon, F., Planquette, H., Pradoux, C., Puigcorbé, V., Quay, P., Queroue, F., Radic, A., Rauschenberg, S., Rehkämper, M., Rember, R., Remenyi, T., Resing, J.A., Rickli, J., Rigaud, S., Rijkenberg, M.J.A., Rintoul, S., Robinson, L.F., Roca-Martí, M., Rodellas, V., Roeske, T., Rolison, J.M., Rosenberg, M., Roshan, S., Rutgers van der Loeff, M.M., Ryabenko, E., Saito, M.A., Salt, L.A., Sanial, V., Sarthou, G., Schallenberg, C., Schauer, U., Scher, H., Schlosser, C., Schnetger, B., Scott, P., Sedwick, P.N., Semiletov, I., Shelley, R., Sherrell, R.M., Shiller, A.M., Sigman, D.M., Singh, S.K., Slagter, H.A., Slater, E., Smethie, W.M., Snaith, H., Sohrin, Y., Sohst, B., Sonke, J.E., Speich, S., Steinfeldt, R., Stewart, G., Stichel, T., Stirling, C.H., Stutsman, J., Swarr, G.J., Swift, J.H., Thomas, A., Thorne, K., Till, C.P., Till, R., Townsend, A.T., Townsend, E., Tuerena, R., Twining, B.S., Vance, D., Velazquez, S., Venchiarutti, C., Villa-Alfageme, M., Vivancos, S.M., Voelker, A.H.L., Wake, B., Warner, M.J., Watson, R., van Weerlee, E., Alexandra Weigand, M., Weinstein, Y., Weiss, D., Wisotzki, A., Woodward, E.M.S., Wu, J., Wu, Y., Wuttig, K., Wyatt, N., Xiang, Y., Xie, R.C., Xue, Z., Yoshikawa, H., Zhang, J., Zhang, P., Zhao, Y., Zheng, L., Zheng, X.Y., Zieringer, M., Zimmer, L.A., Ziveri, P., Zunino, P., Zurbrick, C., 2018. The GEOTRACES Intermediate Data Product 2017. Chem. Geol. 493, 210–223. https://doi.org/10.1016/j.chemgeo.2018.05.040

Schroth, A.W., Crusius, J., Sholkovitz, E.R., Bostick, B.C., 2009. Iron solubility driven by speciation in dust sources to the ocean. Nat. Geosci. 2, 337–340. https://doi.org/10.1038/ngeo501

Sedwick, P.N., Sholkovitz, E.R., Church, T.M., 2007. Impact of anthropogenic combustion emissions on the fractional solubility of aerosol iron: Evidence from the Sargasso Sea. Geochemistry, Geophys. Geosystems 8. https://doi.org/10.1029/2007GC001586

Shelley, R.U., Morton, P.L., Landing, W.M., 2015. Elemental ratios and enrichment factors in aerosols from the US-GEOTRACES North Atlantic transects. Deep. Res. Part II Top. Stud. Oceanogr. 116, 262–272. https://doi.org/10.1016/j.dsr2.2014.12.005

Shelley, R.U., Roca-Martí, M., Castrillejo, M., Masqué, P., Landing, W.M., Planquette, H., Sarthou, G., 2017. Quantification of trace element atmospheric deposition fluxes to the Atlantic Ocean (>40°N; GEOVIDE, GEOTRACES GA01) during spring 2014. Deep. Res. Part I Oceanogr. Res. Pap. 119, 34–49. https://doi.org/10.1016/j.dsr.2016.11.010

Shi, Z., Krom, M.D., Bonneville, S., Benning, L.G., 2015. Atmospheric processing outside clouds increases soluble iron in mineral dust. Environ. Sci. Technol. 49, 1472–1477. https://doi.org/10.1021/es504623x

Sholkovitz, E.R., Sedwick, P.N., Church, T.M., 2009. Influence of anthropogenic combustion emissions on the deposition of soluble aerosol iron to the ocean: Empirical estimates for island sites in the North Atlantic. Geochim. Cosmochim. Acta 73, 3981–4003.

https://doi.org/10.1016/j.gca.2009.04.029
Sholkovitz, E.R., Sedwick, P.N., Church, T.M., Baker, A.R., Powell, C.F., 2012. Fractional solubility of aerosol iron: Synthesis of a global-scale data set. Geochim. Cosmochim. Acta 89, 173–189. https://doi.org/10.1016/j.gca.2012.04.022
Smith, T.E.L., Paton-Walsh, C., Meyer, C.P., Cook, G.D., Maier, S.W., Russell-Smith, J., Wooster, M.J., Yates, C.P., 2014. New emission factors for Australian vegetation fires measured using open-path fourier transform infrared spectroscopy - Part 2: Australian tropical savanna fires. Atmos. Chem. Phys. 14, 11335–11352. https://doi.org/10.5194/acp-14-11335-2014
Srinivas, B., Sarin, M.M., 2013. Atmospheric dry-deposition of mineral dust and anthropogenic trace metals to the Bay of Bengal. J. Mar. Syst. 126, 56–68. https://doi.org/10.1016/j.jmarsys.2012.11.004
Stein, A.F., Draxler, R.., Rolph, G.D., Stunder, B.J.B., Cohen, M.D., Ngan, F., 2015. NOAA's HYSPLIT atmospheric transport and dispersion modeling system. Bull. Amer. Meteor. Soc 96, 2059–2077. https://doi.org/http://dx.doi.org/10.1175/BAMS-D-14-00110.
Stockdale, A., Krom, M.D., Mortimer, R.J.G., Benning, L.G., Carslaw, K.S., Herbert, R.J., Shi, Z., Myriokefalitakis, S., Kanakidou, M., Nenes, A., 2016. Understanding the nature of atmospheric acid processing of mineral dusts in supplying bioavailable phosphorus to the oceans. Proc. Natl. Acad. Sci. 113, 201608136. https://doi.org/10.1073/pnas.1608136113
Strzelec, M., Proemse, B.C., Barmuta, L.A., Gault-Ringold, M., Perron, M.M.G., Desservettaz, M., Boyd, P.W., Schofield, R., Bowie, A.R., 2019a. Atmospheric trace metal deposition from natural and anthropogenic sources in Western Australia. prep.
Strzelec, M., Proemse, B.C., Gault-Ringold, M., Boyd, P.W., Perron, M.M.G., Schofield, R., Ryan, R.G., Ristovski, Z.D., Alroe, J., Humphries, R.S., Keywood, M.D., Ward, J., Bowie, A.R., 2019b. Atmospheric trace metal deposition near the Great Barrier Reef, Australia. prep.
Taylor, M.P., Mackay, A.K., Hudson-Edwards, K.A., Holz, E., 2010. Soil Cd, Cu, Pb and Zn contaminants around Mount Isa city, Queensland, Australia: Potential sources and risks to human health. Appl. Geochemistry 25, 841–855. https://doi.org/10.1016/J.APGEOCHEM.2010.03.003
Titelius, R., 2016. Waroona fire: Australia and global warming. Guard.
Viscarra Rossel, R.A., 2011. Fine-resolution multiscale mapping of clay minerals in Australian soils measured with near infrared spectra. J. Geophys. Res. Earth Surf. 116, 1–15. https://doi.org/10.1029/2011JF001977
Viscarra Rossel, R.A., Chen, C., 2011. Digitally mapping the information content of visible-near infrared spectra of surficial Australian soils. Remote Sens. Environ. 115, 1443–1455. https://doi.org/10.1016/j.rse.2011.02.004
Wagener, T., Guieu, C., Losno, R., Bonnet, S., Mahowald, N.M., 2008. Revisiting atmospheric dust export to the Southern Hemisphere ocean Biogeochemical implications. Global Biogeochem. Cycles 22. https://doi.org/10.1029/2007GB002984
Wang, R., Balkanski, Y., Boucher, O., Bopp, L., Chappell, A., Ciais, P., Hauglustaine, D., Peñuelas, J., Tao, S., 2015. Sources, transport and deposition of iron in the global atmosphere. Atmos. Chem. Phys. 15, 6247–6270. https://doi.org/10.5194/acp-15-6247-2015
Winton, V.H.., Edwards, R., Bowie, A.R., Keywood, M., Williams, A.G., Chambers, S.D., Selleck, P.W., Desservettaz, M., Mallet, M.D., Paton-Walsh, C., 2016. Dry season aerosol iron solubility in tropical northern Australia. Atmos. Chem. Phys. 16, 12829–12848. https://doi.org/10.5194/acp-16-12829-2016
Witt, M.L.I., Mather, T.A., Baker, A.R., De Hoog, J.C.M., Pyle, D.M., 2010. Atmospheric trace metals over the south-west Indian Ocean: Total gaseous mercury, aerosol trace metal

concentrations and lead isotope ratios. Mar. Chem. 121, 2–16. https://doi.org/10.1016/j.marchem.2010.02.005

Wooster, M.J.J., Xu, W., Nightingale, T., 2012. Sentinel-3 SLSTR active fire detection and FRP product: Pre-launch algorithm development and performance evaluation using MODIS and ASTER datasets. Remote Sens. Environ. 120, 236–254. https://doi.org/10.1016/J.RSE.2011.09.033